PLOS GENETICS

RESEARCH ARTICLE

MED19 alters AR occupancy and gene expression in prostate cancer cells, driving MAOA expression and growth under low androgen

Hannah Weber, Rachel Ruoff, Michael J. Garabedian*

Departments of Microbiology and Urology, New York University School of Medicine, New York, New York, United States of America

* michael.garabedian@nyulangone.org

OPEN ACCESS

Citation: Weber H, Ruoff R, Garabedian MJ (2021) MED19 alters AR occupancy and gene expression in prostate cancer cells, driving MAOA expression and growth under low androgen. PLoS Genet 17(1): e1008540. https://doi.org/10.1371/journal.pgen.1008540

Editor: Wilbert Zwart, Netherlands Cancer Institute, NETHERLANDS

Received: November 22, 2019

Accepted: January 4, 2021

Published: January 29, 2021

Data Availability Statement: All relevant data are within the paper and Supporting Information files, with sequencing data generated for this study deposited to the NCBI Gene Expression Omnibus (GEO). The accession for the data sets is available in GEO under accession number GSE161268.

Funding: This work was supported by the NIH grants 5T32GM066704 (HW), T32GM007308 (HW), and R21CA202122 (MJG). https://grants.nih.gov/funding/searchguide/index.html#/ The funders had no role in study design, data

Abstract

Androgen deprivation therapy (ADT) is a mainstay of prostate cancer treatment, given the dependence of prostate cells on androgen and the androgen receptor (AR). However, tumors become ADT-resistant, and there is a need to understand the mechanism. One possible mechanism is the upregulation of AR co-regulators, although only a handful have been definitively linked to disease. We previously identified the Mediator subunit MED19 as an AR co-regulator, and reported that MED19 depletion inhibits AR transcriptional activity and growth of androgen-insensitive LNCaP-abl cells. Therefore, we proposed that MED19 upregulation would promote AR activity and drive androgen-independent growth. Here, we show that stable overexpression of MED19 in androgen-dependent LNCaP cells promotes growth under conditions of androgen deprivation. To delineate the mechanism, we determined the MED19 and AR transcriptomes and cistromes in control and MED19-overexpressing LNCaP cells. We also examined genome-wide H3K27 acetylation. MED19 overexpression selectively alters AR occupancy, H3K27 acetylation, and gene expression. Under conditions of androgen deprivation, genes regulated by MED19 correspond to genes regulated by ELK1, a transcription factor that binds the AR N-terminus to induce select AR target gene expression and proliferation, and genomic sites occupied by MED19 and AR are enriched for motifs associated with ELK1. Strikingly, MED19 upregulates expression of monoamine oxidase A (MAOA), a factor that promotes prostate cancer growth. MAOA depletion reduces androgen-independent growth. MED19 and AR occupy the MAOA promoter, with MED19 overexpression enhancing AR occupancy and H3K27 acetylation. Furthermore, MED19 overexpression increases ELK1 occupancy at the MAOA promoter, and ELK1 depletion reduces MAOA expression and androgen-independent growth. This suggests that MED19 cooperates with ELK1 to regulate AR occupancy and H3K27 acetylation at MAOA, upregulating its expression and driving androgen independence in prostate cancer cells. This study provides important insight into the mechanisms of prostate cancer cell growth under low androgen, and underscores the importance of the MED19-MAOA axis in this process.

collection, analysis, decision to publish, or preparation of the manuscript.

Competing interests: The authors have declared that no competing interests exist.

Author summary

Prostate cancer is one of the most common cancers worldwide, and androgen hormones are essential for prostate cancer growth. Androgens exert their effects through a protein called the androgen receptor (AR), which turns on and off genes that regulate prostate cancer growth. Powerful drugs that block AR action by lowering androgen levels–so-called androgen deprivation therapy—are used to treat prostate cancer patients, and this yields initial success in reducing tumor growth. However, over time, tumors circumvent androgen deprivation therapy and patients relapse; in many cases, this occurs because AR becomes re-activated. The factors responsible for re-activating AR and promoting growth under androgen deprivation are not well understood. Here, we demonstrate that a subunit of the Mediator transcriptional regulatory complex, called MED19, promotes growth of prostate cancer cells under low androgen conditions, mimicking the ability of tumors to grow under androgen deprivation in prostate cancer patients. MED19 promotes androgen-independent growth by working with a transcription factor that interacts with AR, called ELK1, to induce the expression of genes regulated by AR that promote prostate cancer growth. This study provides important insight into how prostate cancer cells can maintain growth under androgen deprivation through MED19.

Introduction

Prostate cells depend on androgens and the androgen receptor (AR) for growth and survival, and AR is a key driver of prostate cancer from early to late stage disease [1]. The mainstay of prostate cancer treatment is androgen deprivation therapy (ADT), to which patients initially respond [2–4]. However, AR re-activation occurs following ADT, giving rise to castration-resistant prostate cancer (CRPC) that can grow in the face of low circulating androgens. Although current treatments, such as enzalutamide and abiraterone, extend survival in CRPC patients, none are curative [2,4–6]. There is a pressing need to better understand the molecular mechanisms behind AR re-activation following ADT.

One important mechanism of AR re-activation with the potential to advance treatment modalities is the upregulation of AR co-regulators [1,7–9]. For example, CBP (CREB binding protein) and p300, both histone acetyl transferases (HATs), are known AR co-regulators that are overexpressed in prostate cancer [10–12]. Targeting these HATs reduces prostate cancer cell growth [13]. BRD4, a chromatin reader that recognizes acetylated histones, is another AR co-regulator that is upregulated in CRPC [14]. Inhibition of BRD4 via a BET inhibitor reduces its interaction with AR, inhibits AR transcriptional activity, and reduces prostate cancer cell growth *in vitro* and *in vivo* [15,16]. Furthermore, BET inhibitors have advanced to clinical trials for CRPC [17].

AR co-regulators implicated in prostate cancer progression also include transcription factors, such as members of the ETS domain family of transcription factors that recognize ETS binding motifs in the genome [7,18]. ETS binding motifs are enriched at AR occupancy sites in prostate cancer cells, and multiple ETS family members are upregulated in prostate cancer [18–22]. In particular, the ETS family member ELK1 was found to interact with the N-terminal domain (NTD) of AR and directly regulate its recruitment to chromatin in prostate cancer cells [23,24]. Inhibition of ELK1 reduces expression of AR target genes and suppresses prostate cancer cell growth [23,24].

However, of the hundreds of proteins that have been identified as AR co-regulators, only a small portion have been definitively linked to disease; furthermore, AR co-regulators function in multi-protein transcriptional complexes [7–9,25]. Therefore, it is important to identify and characterize co-regulators that play a key role in mediating these complexes, are crucial for driving AR transcriptional activity and growth, and are upregulated in prostate cancer.

To this end, our lab previously performed an unbiased, genome-wide siRNA screen for novel AR co-regulators, and identified MED19, a subunit of the middle module of the Mediator complex that functionally bridges promoters and enhancers to connect transcription factors and RNA polymerase II (Pol II) [26,27]. We found that MED19 depletion greatly inhibited AR transcriptional activity and proliferation of LNCaP-abl cells (androgen-independent) and LNCaP cells (androgen-dependent). MED19 mRNA is also upregulated in primary and metastatic prostate cancer, and its abundance correlates with lower overall survival [26,28,29]. From this, we proposed that upregulation of MED19 in prostate cancer cells drives AR activity and androgen independence. However, the mechanism by which MED19 regulates AR activity, particularly under low androgen conditions (as occurs during ADT), as well as the downstream gene targets controlling growth, remained unknown.

In this study we examined the ability of MED19 to confer androgen independence and its effect on gene expression and AR occupancy. We identified the specific gene target, MAOA, and cooperating transcription factor, ELK1, underlying MED19 regulation of androgen-independent growth.

Results

MED19 overexpression promotes androgen independence and confers a growth advantage to prostate cells

To determine if MED19 is sufficient to convert androgen-dependent prostate cancer cells to androgen independence, we stably overexpressed MED19 by lentiviral transduction in the prototypical androgen-dependent LNCaP cell line (MED19 LNCaP cells) (S1 Fig). As a control, we also created the parental LNCaP cells stably expressing the empty lentiviral vector (control LNCaP cells). Both lines represent a pool of cells. We found by immunofluorescence that the MED19 LNCaP cells uniformly express MED19 at roughly comparable levels on a per cell basis with expression in both the nucleus and cytoplasm (S2A Fig). We did not observe any obvious morphological changes in the MED19 LNCaP cells compared to control cells (S2B Fig). In the MED19 LNCaP cells there was a clear increase in the protein abundance of overexpressed MED19 relative to endogenous MED19 in control cells (S2C Fig). We compared their proliferation under androgen-deprived conditions in 2D culture; by colony formation, which measures the survival and replicative potential of individual cancer cells; and by spheroid formation, a 3D cell culture condition more representative of a tumor.

In contrast to control LNCaP cells, MED19 LNCaP cells showed robust proliferation in 2D culture, increased colony formation, and larger spheroid formation, when cultured in media depleted of steroids (Fig 1A–1C). This demonstrates that expression of MED19 is sufficient to promote androgen independence in prostate cancer cells. This is consistent with our previous findings that MED19 in androgen-independent LNCaP-abl cells is necessary for growth. MED19 overexpression also conferred a growth advantage, albeit less striking, when the cells were cultured in complete media containing endogenous steroids (Fig 1D–1F). This is also consistent with reports from our lab and others demonstrating that depletion of MED19 inhibits LNCaP cell growth in the presence of androgens [26,30].

We also examined if upregulation of MED19 could promote the proliferation of other early stage prostate cancer cell lines. Indeed, we found that overexpression of MED19 increased

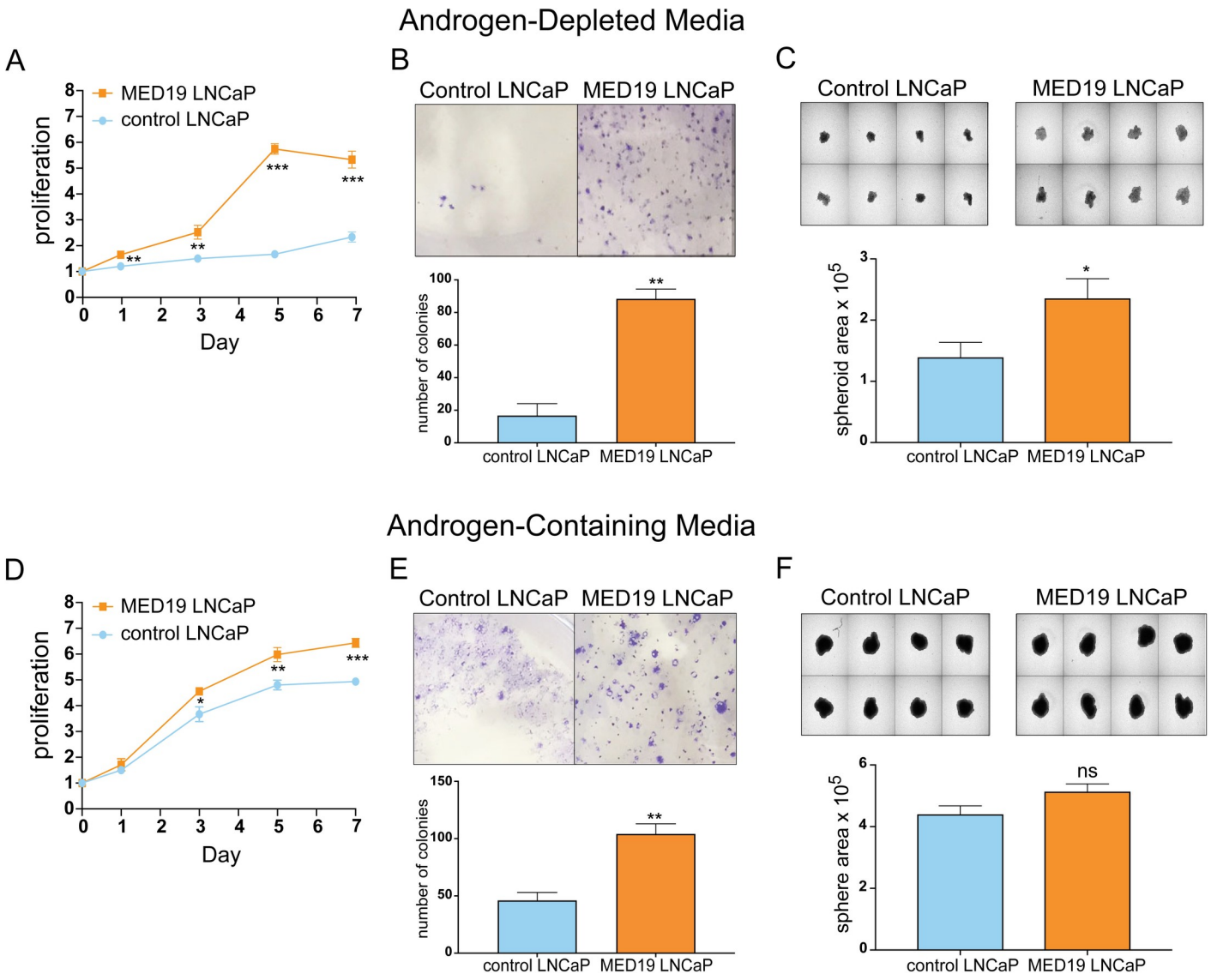

Fig 1. MED19 overexpression confers a growth advantage and enables androgen-independent growth of LNCaP cells. LNCaP cells stably overexpressing MED19 (MED19 LNCaP cells) and LNCaP cells expressing the empty lentiviral vector (control LNCaP cells) were cultured in media depleted of androgens by addition of FBS charcoal-stripped of steroids (A, B, C) or media containing androgens by addition of standard FBS (D, E, F). A) and D) Proliferation was measured over 7 days and is expressed as fold change in relative fluorescent units (RFU), normalized to Day 0. B) and E) Colony formation was evaluated by culturing MED19 LNCaP cells and control LNCaP cells at low density for 11 days, fixing and staining with crystal violet, and quantifying the number of colonies per field (n = 3). C) and F) Spheroid formation was evaluated by culturing cells on low attachment plates for 10 days and quantifying average spheroid area. Experiments were performed in biological triplicate, with representative results shown. $^{*}p < 0.05$; $^{**}p < 0.01$; and $^{***}p < 0.001$. ns = not significant.

https://doi.org/10.1371/journal.pgen.1008540.g001

proliferation in non-malignant RWPE-1 cells (Fig 2A), but did not affect the growth of RWPE-2 cells, which are a malignant derivative of RWPE-1 cells, transformed with RAS (Fig 2B) [31]. This is in spite of similar levels of MED19 protein expressed in RWPE-1 cells and RWPE-2 cells (S3 Fig). Furthermore, a murine prostate stem cell (MSC) line transformed with a constitutively active myristoylated AKT grew markedly faster upon MED19 overexpression compared to its control counterpart (Fig 2C) [32]. This was recapitulated in a xenograft model, where the MED19-overexpressing cells produced larger tumors than control cells (Fig 2D). Whereas sections from both control MSC and MED19 MSC tumors had similar phospho-AKT (pAKT) levels by immunohistochemistry (IHC) (S4A Fig), MED19 MSC-derived

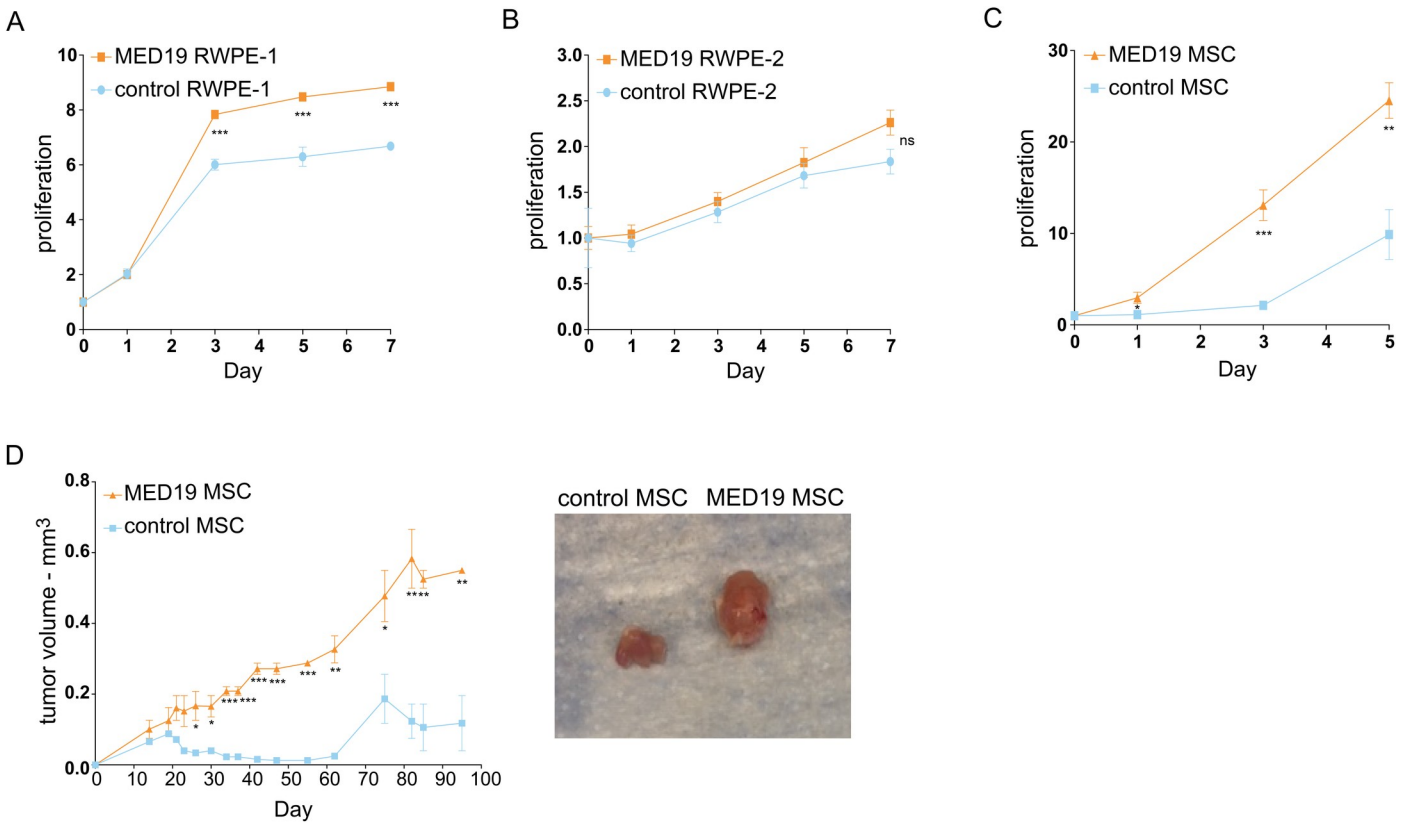

Fig 2. MED19 overexpression promotes proliferation *in vitro* in non-malignant RWPE-1 cells and *in vitro* and *in vivo* in mouse prostate stem cells. A) RWPE-1, B) RWPE-2, or C) mouse stem cells (MSC) expressing a constitutively active myristoylated AKT, and stably overexpressing MED19 (MED19 RWPE-1/RWPE-2/MSC) or control empty vector (control RWPE-1/RWPE-2/MSC), were cultured in their standard media. A-C) Proliferation was measured over 5 days for the MSC, which have a rapid doubling time, or 7 days for RWPE-1 cells and RWPE-2 cells, and is expressed as fold change in relative fluorescent units (RFU) normalized to Day 0. Experiments were performed in biological duplicate, with representative results shown. D) MED19 MSC or control MSC were injected into the flanks of Nu/J mice and tumor volume was measured over 95 days (2 mice per group). Representative images of tumors taken at time of sacrifice are shown. $^{*}p < 0.05$; $^{**}p < 0.01$; and $^{***}p < 0.001$. ns = not significant.

https://doi.org/10.1371/journal.pgen.1008540.g002

tumors displayed clusters of cells staining strongly for phospho-ERK (pERK) that were not present in tumors from the control MSC (S4B Fig). This suggests sustained ERK activation in a subset of cells within the tumor, although the identity of these cells remains to be determined. We also assessed by IHC the abundance of AR, as well as Ki-67 as a marker of proliferation. As expected, we found higher levels of Ki-67 (S4C Fig) in the tumors derived from MED19 MSC cells compared to control MSC, consistent with the increased tumor size of MED19 MSC xenografts. Overall AR abundance was comparable in control MSC and MED19 MSC, although there appeared to be more nuclear AR in the tumors from MED19 MSC (S4D Fig), suggestive of active AR signaling. This corroborates the growth advantage of MED19 overexpression found in LNCaP cells.

Altogether, this indicates a role for MED19 in conversion of early stage cells to aggressive growth and androgen independence.

MED19 depends on AR activity for its growth advantage but does not alter AR expression

As AR amplification is a common mechanism to achieve androgen independence, we evaluated the mRNA and protein levels of AR with MED19 overexpression in LNCaP cells. We

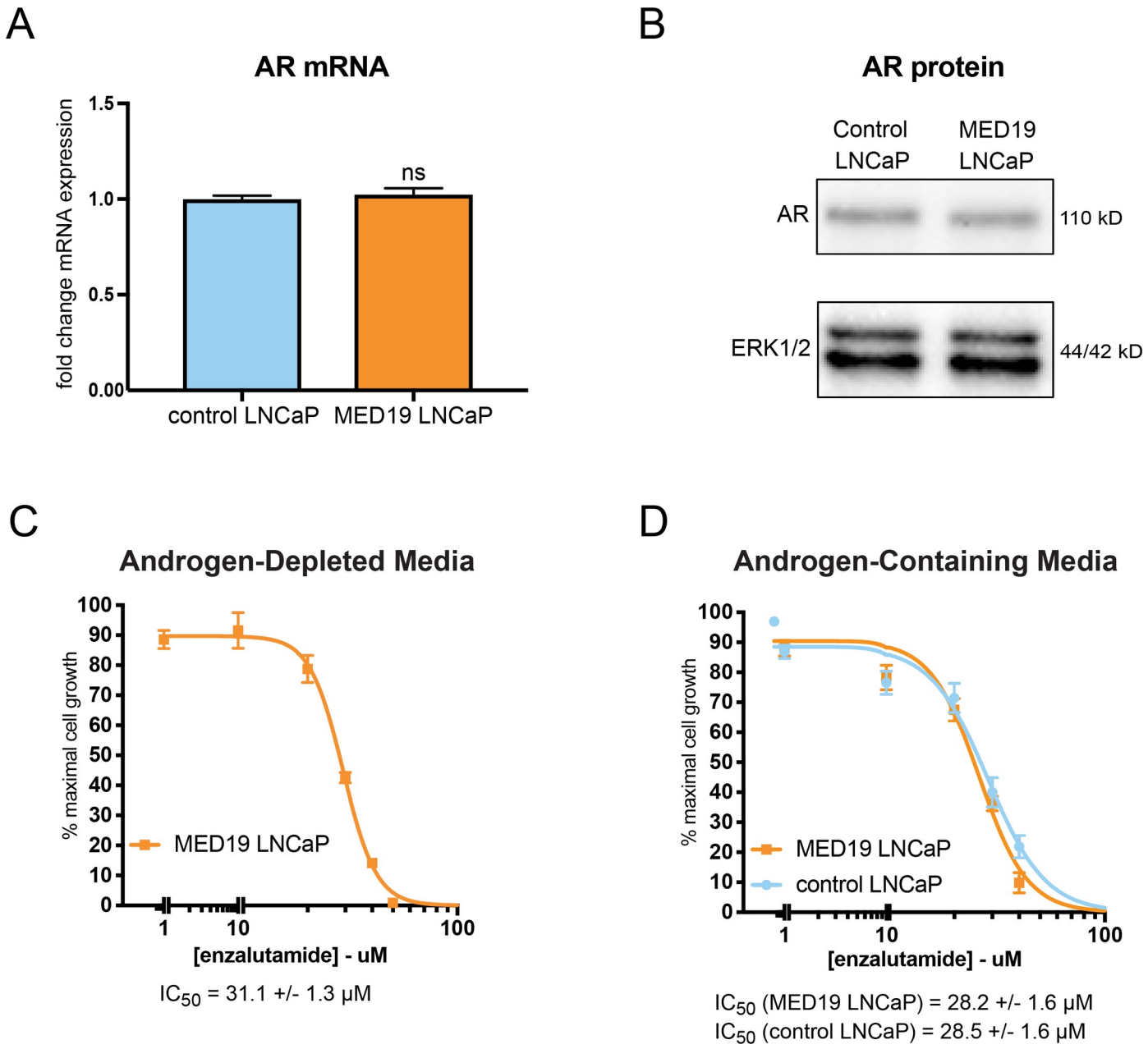

Fig 3. MED19 LNCaP cells depend on AR transcriptional activity for androgen-independent growth and do not have altered expression of AR. A) RNA was extracted from control LNCaP and MED19 LNCaP cells cultured under androgen deprivation for 3 days, and AR mRNA measured by qPCR (fold change mRNA expression normalized to RPL19, with AR mRNA expression in control LNCaP cells set as "1") ns = not significant. B) Total protein lysate was collected and probed for AR protein levels by western blot. ERK1/2 was used as a loading control. C) and D) MED19 LNCaP cells were treated with enzalutamide (0–80 μM) in C) androgen-depleted media, or D) androgen-containing media, alongside control LNCaP cells. Proliferation was measured over 7 days. Percent cell growth at day 7 is normalized to vehicle treatment (0 μM, 100%). The IC_{50} from three experiments is shown. Experiments were performed in biological triplicate, with representative results shown.

https://doi.org/10.1371/journal.pgen.1008540.g003

found that AR mRNA and protein were unchanged in MED19 LNCaP cells compared to control LNCaP cells under androgen deprivation (Fig 3A and 3B). MED19 overexpression also did not induce expression of AR-V7, a constitutively active splice variant of AR lacking the ligand binding domain that can drive androgen independence in prostate cancer (S5 Fig) [33].

We then examined the reliance of MED19 LNCaP cells on AR for their androgen-independent growth by determining their sensitivity to enzalutamide, an AR antagonist that reduces AR transcriptional activity in part by preventing AR nuclear accumulation [34]. Enzalutamide inhibited the proliferation of MED19 LNCaP cells both in the presence and absence of androgens, indicating that the growth advantage conferred by MED19 requires AR transcriptional activity (Fig 3C and 3D). We confirmed these results by siRNA depletion of AR, which also reduced androgen-independent and androgen-dependent proliferation of MED19 LNCaP cells (S6A–S6C Fig).

Prior to embarking on a genome-wide assessment of the effect of MED19 overexpression on gene expression in LNCaP cells, we examined a select set of androgen-regulated genes by qPCR in control LNCaP cells *versus* MED19 LNCaP cells cultured under androgen deprivation and treated with vehicle (basal) or R1881 (androgen), a synthetic AR agonist. MED19 overexpression upregulated both basal and androgen-dependent expression of the cell cycle regulators *UBE2C* and *MYC* (S7A Fig). MED19 overexpression also reduced by half the androgen-dependent induction of *PSA* mRNA (S7B Fig). This was accompanied by a corresponding reduction in the nascent *PSA* RNA, indicating that the changes in mRNA expression upon androgen treatment occurred at the transcriptional level (S7B Fig). MED19 overexpression had a negligible effect on the induction by androgen of other AR target genes, including *FKBP5* (S7C and S7D Fig). These findings suggest that MED19 expression selectively affects AR target gene expression.

MED19 regulates gene expression by altering AR occupancy and H3K27 acetylation at target genes

MED19 relies on the transcriptional activity of AR for its growth advantage, and as part of the Mediator complex controls gene expression through transcription factor, co-regulator, and histone modifying complex recruitment. Thus, we evaluated the effect of overexpressed MED19 on gene expression, AR occupancy, and H3K27 acetylation under androgen deprivation and in response to androgens, with a particular focus to identify the specific gene expression and AR occupancy changes driving androgen independence. To this end, we performed RNA sequencing (RNA-seq) and ChIP sequencing (ChIP-seq) studies for FLAG-tagged MED19, AR, and H3K27 acetylation in MED19 LNCaP cells and control LNCaP cells cultured under androgen deprivation and treated with vehicle (androgen-deprived conditions) or R1881 (androgen-treated conditions).

Global AR occupancy under androgen deprivation, as measured by total number of and individual level of occupancy at AR sites in published ChIP-seq studies, is low compared to androgen treatment. We speculated that MED19 may alter AR activity under androgen deprivation by modulating AR at low occupancy sites. Therefore, we included in our ChIP-seq study all AR-specific sites, including those with low occupancy in androgen-deprived conditions. We used rigorous quality controls to maximize capture of AR sites and ensure strict specificity to AR occupancy (see detailed ChIP-seq section under Materials and Methods) (S8 Fig and S7 Table).

Under androgen deprivation, there was a striking and very selective change in the gene expression profile with MED19 overexpression, with a total of 151 genes altered (76 genes upregulated and 75 genes downregulated, fold change$\geq$1.5 and p-adj$\leq$0.05; *UBE2C* and *MYC* fell below the 1.5-fold cut-off) (Fig 4A and S1 Table). This was accompanied by a selective shift in the AR cistrome (~12% of total AR sites are occupied only in control LNCaP cells or only in MED19 LNCaP cells), without a global change in the total number of sites occupied by AR (Fig 4A). As expected, with androgen treatment, the total number of AR sites increased (Fig

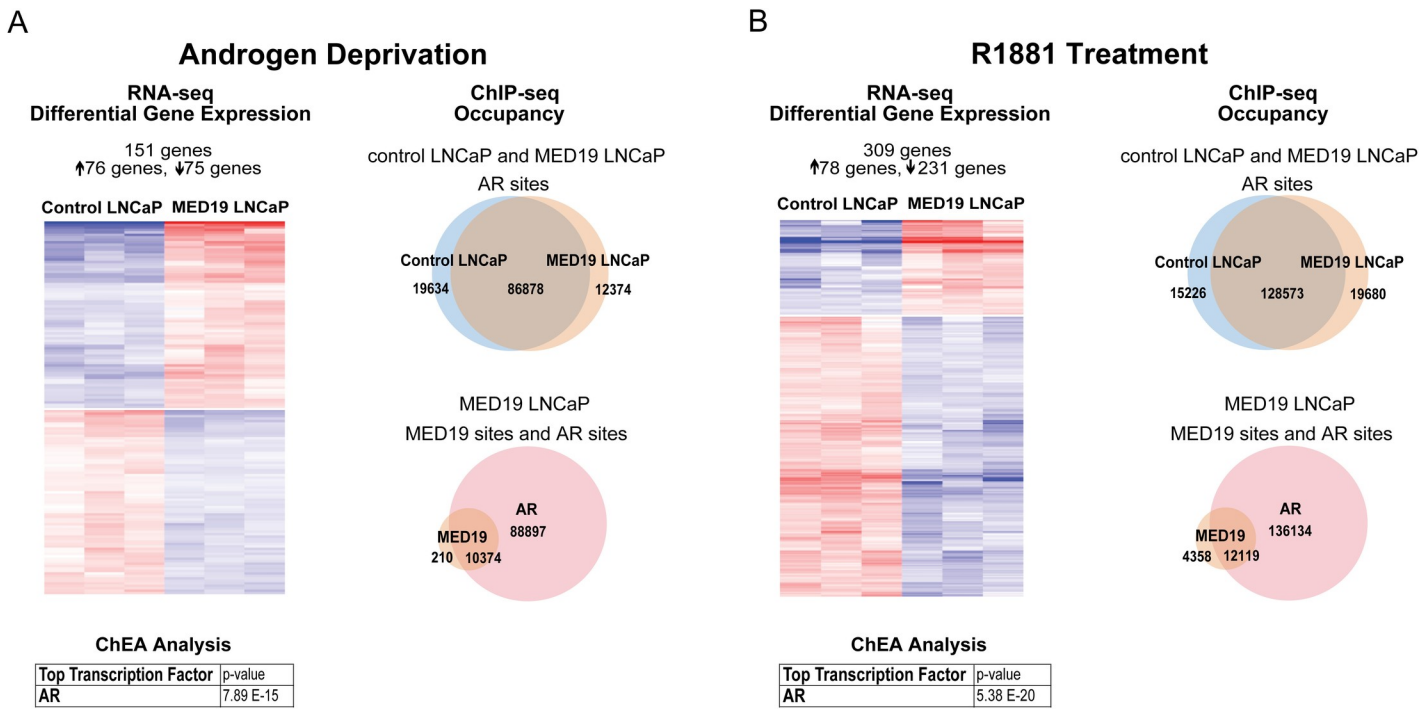

Fig 4. MED19 overexpression causes a selective shift in gene expression and in the AR cistrome under androgen deprivation and with R1881 treatment. MED19 LNCaP cells and control LNCaP cells were cultured under androgen deprivation for 3 days, and cells were treated with ethanol vehicle or R1881 (10 nM for 16 h for RNA-seq and 100 nM for 4 h for ChIP-seq). RNA-seq with ribodepletion was performed in biological triplicate. ChIP-seq for FLAG-MED19, AR, and H3K27ac was performed in biological triplicate, with the exception of ChIP-seq for AR in control LNCaP cells + R1881, where one sample was excluded from the analyses because of low signal. A) (Left) Heatmap of differentially expressed genes with MED19 overexpression (fold change ≥1.5, p-adj ≤0.05) for androgen deprivation, associated with AR as the top regulatory transcription factor from ChEA. (Right) Number and overlap of occupancy sites under androgen deprivation for AR in control LNCaP cells and MED19 LNCaP cells (top) and for AR and MED19 in MED19 LNCaP cells (bottom). B) (Left) Heatmap of differentially expressed genes with MED19 overexpression (fold change ≥1.5, p-adj ≤0.05) for R1881 treatment, associated with AR as the top regulatory transcription factor from ChEA. (Right) Number and overlap of occupancy sites with R1881 treatment for AR in control LNCaP cells and MED19 LNCaP cells (top) and for AR and MED19 in MED19 LNCaP cells (bottom).

https://doi.org/10.1371/journal.pgen.1008540.g004

5A and 5B). There was a selective shift in the AR cistrome when MED19 was overexpressed in the presence of androgens as well (Fig 4B). There was also a shift in gene expression: 309 genes were differentially expressed with MED19 overexpression in the presence of androgens (78 genes upregulated and 231 downregulated, fold change≥1.5 and p-adj≤0.05) (Fig 4B and S2 Table).

Of these 309 genes, 82 were also differentially expressed in the absence of androgens (~50% of total genes differentially expressed in the absence of androgens) (S1 and S2 Tables). This holds for MED19 occupancy as well: the total number of MED19 sites increased with androgen treatment, with ~50% of the sites occupied in the absence of androgens also occupied in the presence of androgens (Fig 5B). This indicates that there is partial overlap in MED19 regulation of gene expression and AR activity in the absence and presence of androgens, consistent with the differential growth advantage in the absence and presence of androgens when MED19 is overexpressed.

MED19 occupancy in the absence and presence of androgens corresponds almost entirely with AR occupancy, with virtually every gene differentially expressed in MED19 LNCaP cells occupied by AR, and many (the majority in the absence of androgens) also occupied by MED19, indicating direct regulation by MED19 (Fig 4A and 4B, S6 Table). In fact, most of the MED19-regulated genes are androgen-responsive, and many have been reported as AR target

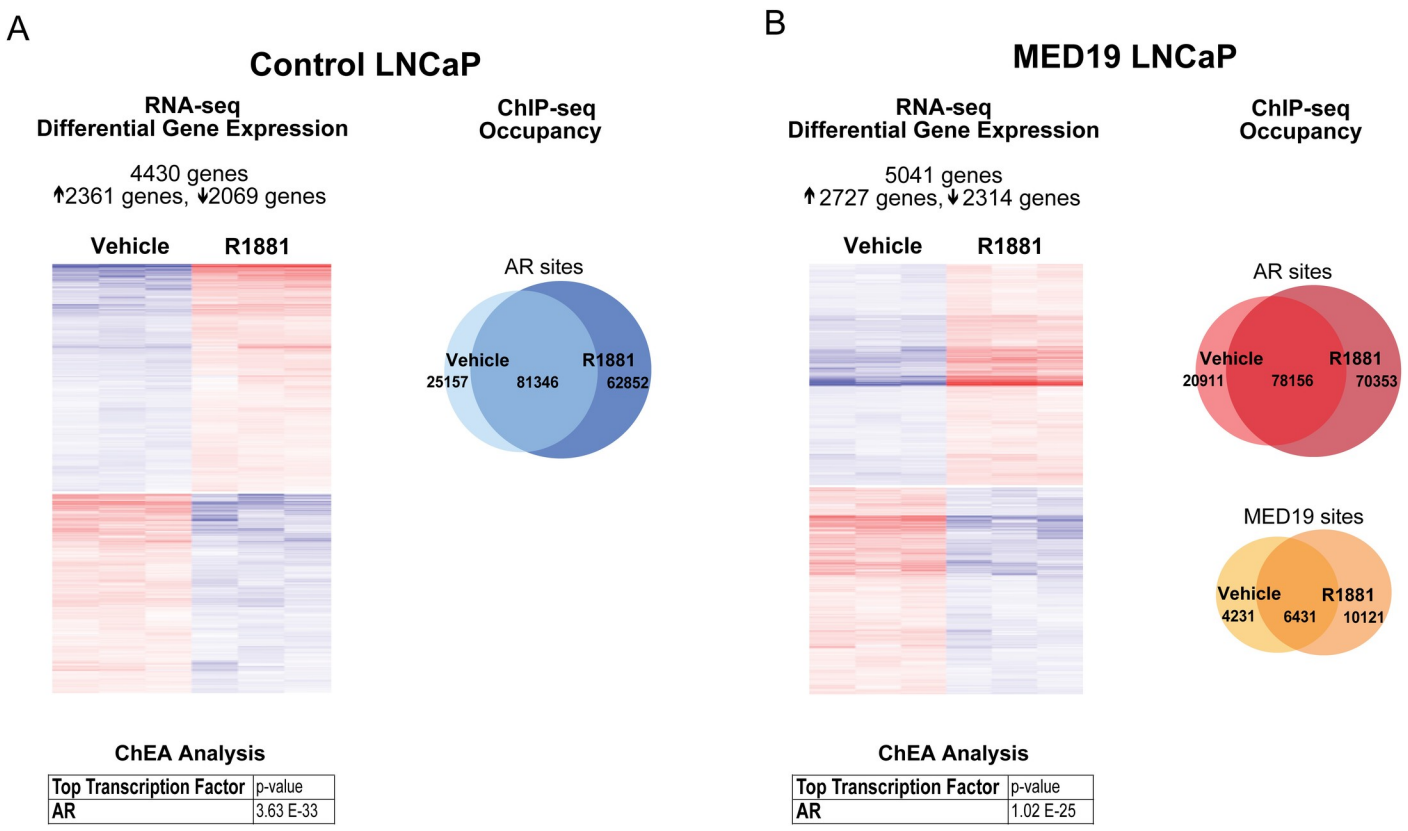

Fig 5. MED19 overexpression alters the response to androgens. MED19 LNCaP cells and control LNCaP cells were cultured under androgen deprivation for 3 days, and cells were treated with ethanol vehicle or R1881 (10 nM for 16 h for RNA-seq and 100 nM for 4 h for ChIP-seq). RNA-seq with ribodepletion was performed in biological triplicate. ChIP-seq for FLAG-MED19, AR, and H3K27ac was performed in biological triplicate, with the exception of ChIP-seq for AR in control LNCaP cells + R1881, where one sample was excluded from the analyses because of low signal. A) (Left) Heatmap of differentially expressed genes (fold change ≥1.5, p-adj ≤0.05) for control LNCaP cells treated with R1881 vs. vehicle, associated with AR as the top regulatory transcription factor from ChEA. (Right) Number and overlap of occupancy sites for R1881 vs. vehicle treatment for AR in control LNCaP cells. B) (Left) Heatmap of differentially expressed genes (fold change ≥1.5, p-adj ≤0.05) for MED19 LNCaP cells treated with R1881 vs. vehicle, associated with AR as the top regulatory transcription factor from ChEA. (Right) Number and overlap of occupancy sites for R1881 vs. vehicle treatment for AR (top) and for MED19 (bottom) in MED19 LNCaP cells.

https://doi.org/10.1371/journal.pgen.1008540.g005

genes (S1 and S2 Tables). AR was also the top predicted regulatory transcription factor candidate using Chromatin immunoprecipitation Enrichment Analysis (ChEA) (Fig 4A and 4B, S1 and S2 Tables). This confirms that MED19 regulation of gene expression is driven by AR.

In response to androgen treatment, ~4,500 genes in control LNCaP cells and ~5,000 genes in MED19 LNCaP cells were differentially expressed (≥1.5-fold, p-adj≤0.05), and, as expected, AR was the top transcription factor from ChEA analysis for both (Fig 5A and 5B, S3 and S4 Tables). This included expected changes in canonical AR target genes, such as induction of *PSA* and *FKBP5* (S9 Fig). Some genes were differentially expressed in response to androgens uniquely to control LNCaP cells (645 genes) or to MED19 LNCaP cells (1,250 genes), comprising ~15 or ~25% of the total genes differentially expressed in response to androgens in control LNCaP cells or MED19 LNCaP cells, respectively, indicating that MED19 alters which genes AR regulates in response to androgens (S5 Table).

MED19 appears mainly to modulate the response of canonically androgen-regulated genes: the top 100 androgen-induced and androgen-repressed genes almost all overlapped between MED19 LNCaP cells and control LNCaP cells, with MED19 overexpression augmenting the response to androgen for some genes, and reducing the response to androgen for others (S5

Table). However, the overall response to androgens does not appear to markedly differ with MED19 overexpression, and differential gene expression with MED19 overexpression in the presence and absence of androgens is very selective (Figs 4 and 5). This indicates that MED19 does not alter the entire AR-regulated transcriptome, nor the global response to androgens (Figs 4 and 5). Overall, this suggests that MED19 alters the cellular response to androgens in a specific manner, consistent with the growth advantage conferred by MED19 overexpression in the presence of androgens.

Although AR occupies unique sites in MED19 LNCaP cells, the majority of genes altered with MED19 overexpression contain AR sites shared by control LNCaP cells and MED19 LNCaP cells (S10 Fig and S6 Table). What we observed at a number of these sites was a change in the level of AR occupancy and/or H3K27 acetylation beyond a "present/absent" or "on/off" binary. These subtle changes in gene occupancy corresponded with MED19 activation or repression of genes from the RNA-seq study, indicating that MED19 alters gene expression through small shifts in AR occupancy (S10A and S10C Fig) and H3K27 acetylation (S10B and S10D Fig). We also observed that the changes in AR occupancy and H3K27 acetylation, like the changes in gene expression with MED19 overexpression, did not simply mimic the changes that occurred with androgen treatment.

For example, LRRTM3 (Leucine Rich Repeat Transmembrane Neuronal 3) is one of the most upregulated genes upon MED19 overexpression under androgen deprivation, while androgen treatment suppresses LRRTM3 expression (Figs 6A and S11A). With MED19 overexpression, there is a clear increase in AR occupancy and H3K27 acetylation at several regulatory intronic sites at LRRTM3, with MED19 occupancy at one of these sites (Figs 6B and S11B). Conversely, androgen treatment reduces H3K27 acetylation and alters AR occupancy (S11B Fig). In contrast, MAST4 is one of the most downregulated genes with MED19 overexpression under androgen deprivation, and is also suppressed by androgen treatment (S12A Fig). There is a clear reduction in H3K27 acetylation adjacent to the MAST4 promoter with MED19 overexpression and with androgen treatment. MED19 overexpression and androgen treatment induce a reorganization of AR occupancy (including a site of occupancy with MED19), though the former does not exactly mimic the latter (S12B Fig). Thus, it appears that AR occupancy at specific targets is altered by MED19 overexpression. This may be responsible for the changes in gene expression and attendant effects on cell proliferation.

We wanted to determine the specific gene targets altered by MED19 overexpression that were responsible for promoting androgen-independent growth. We decided to focus on genes upregulated by MED19 overexpression under androgen deprivation, which could be depleted to inhibit androgen-independent growth. Given that LRRTM3 appears to be a direct target of MED19, with changes in AR occupancy that correlated with a large upregulation in expression, we tested its effect on proliferation. However, LRRTM3 depletion had very little effect on androgen-independent growth (S11C Fig). Although we cannot exclude the possibility that the knockdown of LRRTM3 was inefficient, the positive control KIF11, a motor protein required for mitosis, showed a potent decrease in cell proliferation (S11C Fig). Furthermore, LRRTM3 has no published connection to AR or prostate cancer. Therefore, we pursued gene targets occupied by MED19 and AR with an established connection to AR, preferably AR target genes, and known to play a role in prostate cancer proliferation.

MED19 upregulates expression and promotes AR occupancy and H3K27 acetylation at MAOA, which is required for androgen-independent growth

One target that fulfilled these criteria is MAOA (monoamine oxidase A). MAOA is a mitochondrial enzyme that degrades monoamine neurotransmitters and dietary amines and

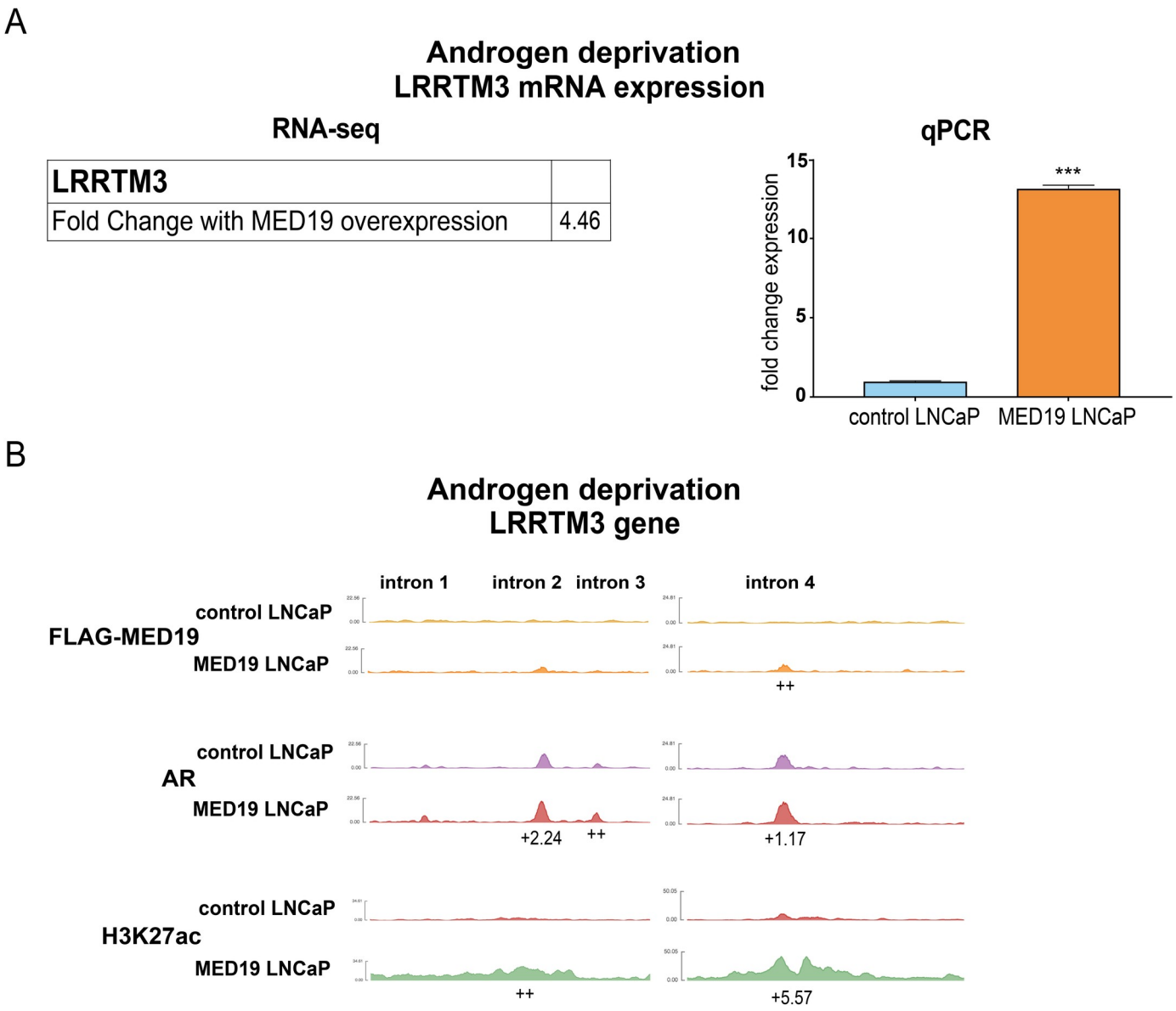

Fig 6. MED19 occupies gene targets like LRRTM3 under androgen deprivation and alters mRNA expression, AR occupancy, and H3K27 acetylation. MED19 LNCaP cells and control LNCaP cells were cultured under androgen deprivation for 3 days and treated with ethanol vehicle (shown) or R1881 (10 nM for 16 h for RNA-seq and 100 nM for 4 h for ChIP-seq; shown in S11 Fig). RNA-seq with ribodepletion was performed in biological triplicate. ChIP-seq for FLAG-MED19, AR, and H3K27ac was performed in biological triplicate, with the exception of ChIP-seq for AR in control LNCaP cells + R1881, where one sample was excluded from the analyses because of low signal. A) Fold change mRNA expression from RNA-seq, and qPCR validation of upregulation of LRRTM3 mRNA expression under androgen deprivation (performed in biological triplicate with representative results shown; fold change expression normalized to RPL19 with LRRTM3 mRNA expression in control LNCaP cells set as "1"). ***$p < 0.001$. B) ChIP-seq tracks (representative results) for FLAG-MED19, AR, and H3K27ac under androgen deprivation shown for intronic regions of LRRTM3. Fold change (up (+) or down (-)) in occupancy scores for MED19 LNCaP cells compared to control LNCaP cells shown for each peak (see S6 Table for all occupancy scores). ++ indicates positive occupancy score in MED19 LNCaP cells and a score of zero in control LNCaP cells;—indicates an occupancy score of zero in MED19 LNCaP cells and a positive score in control LNCaP cells.

https://doi.org/10.1371/journal.pgen.1008540.g006

produces hydrogen peroxide. It has a well-established role in promoting aggressive prostate cancer cell growth, invasion, and metastasis [35–38]. MAOA is also reported as an AR target gene with an androgen response element (ARE) in its promoter [39]. Indeed, MAOA expression increased in control LNCaP cells in response to R1881, which was comparable to the increase in expression in MED19 LNCaP cells under androgen deprivation (Figs 7A and S13A,

S1 and S3 Tables). This indicates that for MAOA expression, MED19 overexpression under androgen deprivation recapitulates the effects of androgen activation.

Indeed, AR occupies the promoter and 5' UTR of MAOA, with increased and reorganized occupancy when MED19 is overexpressed and when the cells are treated with R1881 (Figs 7B and S13B). ChIP-qPCR for the MAOA promoter region overlapping with the published ARE confirmed MED19 and AR occupancy, with increased AR occupancy and H3K27 acetylation with MED19 overexpression and with R1881 treatment (Figs 7C and S13C). To determine whether MED19 activation of MAOA was responsible for androgen-independent growth, we depleted MAOA in MED19 LNCaP cells under androgen deprivation and measured proliferation. MAOA depletion reduced growth by ~50% (Fig 7D and 7E). Interestingly, from the RNA-seq study, MAOA is not differentially upregulated with MED19 overexpression in the presence of androgens, which is consistent with the relatively smaller growth advantage of MED19 overexpression when androgens are present (S13A Fig, S1–S4 Tables).

ELK1 is enriched at MED19 and AR occupied sites and upregulated targets, driving MAOA expression and androgen-independent growth

Since increased or decreased AR recruitment corresponded to activation or repression of target genes as a function of MED19 overexpression, and given that AR works in concert with other transcription factors to control gene expression, we determined the identity of other transcription factor binding motifs associated with AR and MED19 occupancy. We were particularly interested in identifying any transcription factors uniquely enriched in MED19 LNCaP cells under androgen deprivation, that correlated with MED19 occupancy, and would have an established connection to prostate cancer and regulation of MAOA.

FOXA1 and FOXM1 were the most enriched transcription factor motifs for AR occupancy in control LNCaP cells and MED19 LNCaP cells, in the absence or presence of androgens, as well as for MED19 occupancy in the absence or presence of androgens (S14 Fig). This is consistent with the well-established role of FOXA1 as a major AR co-regulator and pioneer factor in prostate cancer cells, and the emerging role of FOXM1 in this capacity as well [40–42]. This is also consistent with the RNA-seq analysis and the vast majority of MED19 sites overlapping with AR sites. However, FOXA1- and FOXM1-mediated recruitment of AR seems unlikely to be the dominant mechanism by which overexpressed MED19 promotes gene expression changes, given that FOXA1 and FOXM1 sites are highly enriched in both MED19 LNCaP cells and control LNCaP cells in all conditions (S14 Fig).

We then focused on the intersection between MED19 and AR occupancy at sites engaged by AR *uniquely* in MED19 LNCaP cells. Under androgen deprivation, we found that the most enriched motif corresponded to ELK1 (Fig 8A). ELK1 is an ETS transcription factor and AR co-regulator that promotes growth in prostate cancer cells and regulates ligand-independent recruitment of AR to chromatin through interaction with the AR NTD [23,24]. Several other members of the ETS family of transcription factors were enriched under androgen deprivation, as well as with androgen treatment (Figs 8A and S15A). In the presence of androgens, the most enriched motif corresponded not to ELK1 but to SP1, an AR-interacting protein upregulated in prostate cancer (S15A Fig) [43]. SP1 is reported to promote AR target gene expression in response to androgens and to occupy sites near gene promoters [44,45]. This confirms that MED19 likely regulates AR occupancy and activity at its upregulated targets through different mechanisms in the absence and presence of androgens.

Interestingly, although sites of AR (and MED19) occupancy in MED19 LNCaP cells and in control LNCaP cells, in the presence and absence of androgens, were enriched for ARE and other canonical AR-related motifs (i.e. ARE half-site and FOXA1:AR motifs), as expected, this

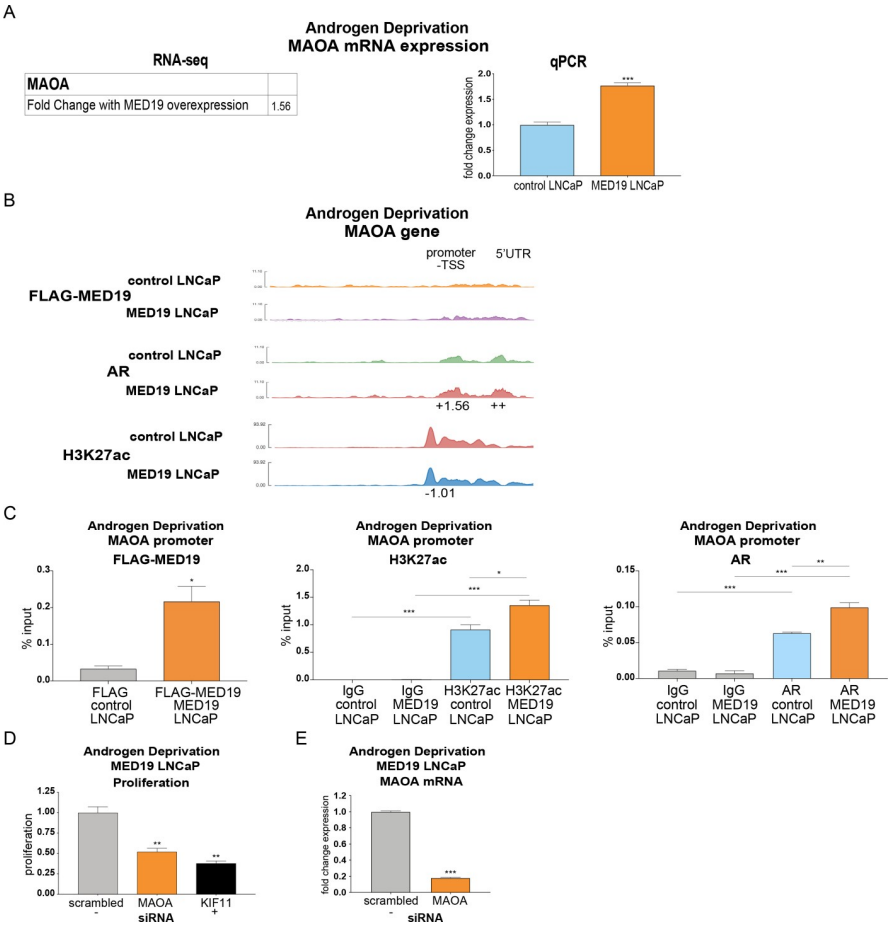

Fig 7. MED19 promotes AR occupancy and H3K27 acetylation at MAOA under androgen deprivation, which controls androgen-independent growth. MED19 LNCaP cells and control LNCaP cells were cultured under androgen deprivation for 3 days and treated with ethanol vehicle (shown) or R1881 (10 nM 16 h for RNA-seq and 100 nM for 4 h for ChIP-seq; shown in S13 Fig). RNA-seq with ribodepletion was performed in biological triplicate. ChIP-seq for FLAG-MED19, AR, and H3K27ac was performed in biological triplicate, with the exception of ChIP-seq for AR in control LNCaP cells + R1881, where one sample was excluded from the analyses because of low signal. A) Fold change mRNA expression from RNA-seq, and qPCR validation of upregulation of MAOA mRNA expression under androgen deprivation (performed in biological triplicate with representative results shown; fold change expression normalized to RPL19 with MAOA mRNA expression in control LNCaP cells set as "1"). B) ChIP-seq tracks (representative results) for FLAG-MED19, AR, and H3K27ac under androgen deprivation shown for promoter region of MAOA. Fold change (up (+) or down (-)) in occupancy scores for MED19 LNCaP cells compared to control LNCaP cells shown for each peak (see S6 Table for all occupancy scores). ++ indicates positive occupancy score in MED19 LNCaP cells and a score of zero in control LNCaP cells;—indicates an occupancy score of zero in MED19 LNCaP cells and a positive score in control LNCaP cells. C) ChIP-qPCR for FLAG-MED19, AR, and H3K27ac at the MAOA promoter overlapping with published ARE. Experiment was performed in duplicate, with representative results shown. D) MAOA was depleted by siRNA and proliferation of MED19 LNCaP cells in androgen-depleted media was evaluated after 7 days, normalized to proliferation with scrambled siRNA treatment (negative control, light grey). KIF11 knockdown is included as a positive control (black). Experiment was performed in biological duplicate, with representative results shown. E) Validation of MAOA knockdown, with MAOA depleted by siRNA and mRNA expression of MAOA in MED19 LNCaP cells cultured in androgen-depleted media measured after 5 days (fold change expression normalized to RPL19, with MAOA mRNA expression with scrambled siRNA treatment set as "1"). $^{*}p < 0.05$; $^{**}p < 0.01$; and $^{***}p < 0.001$.

https://doi.org/10.1371/journal.pgen.1008540.g007

enrichment was reduced under androgen deprivation (S16 Fig). In addition, these motifs were absent at sites of MED19 and AR occupancy in MED19 LNCaP cells where AR was present only in MED19 LNCaP cells. This would be consistent with the ability of ELK1 to act as an AR tethering protein to promote AR recruitment to non-canonical sites.

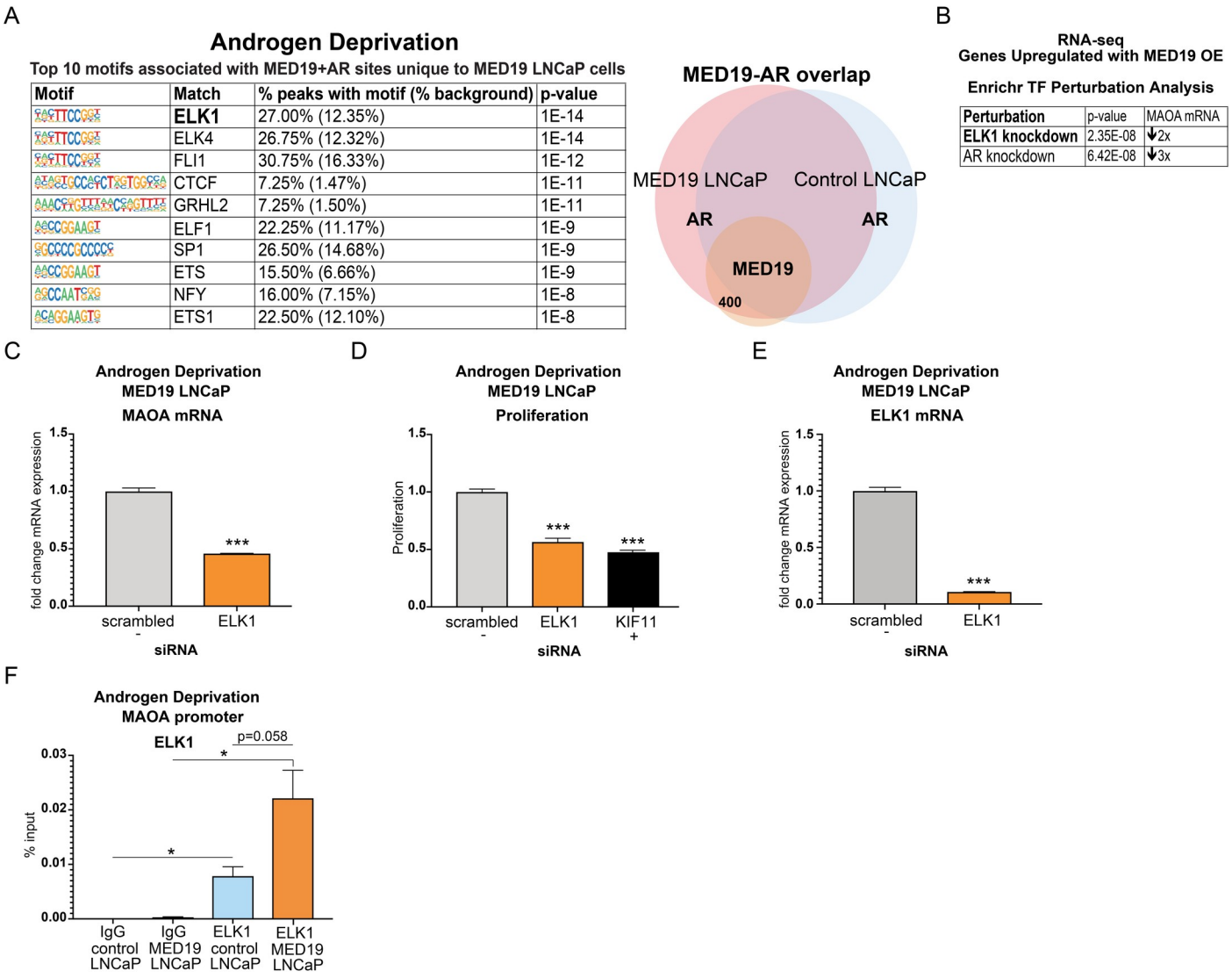

Fig 8. ELK1 is enriched at sites of AR and MED19 occupancy unique to MED19 LNCaP cells under androgen deprivation, occupies the MAOA promoter, and controls MAOA expression and androgen-independent growth. MED19 LNCaP cells and control LNCaP cells were cultured under androgen deprivation for 3 days and treated with ethanol vehicle. RNA-seq with ribodepletion was performed in biological triplicate. ChIP-seq for FLAG-MED19, AR, and H3K27ac was performed in biological triplicate, with the exception of ChIP-seq for AR in control LNCaP cells + R1881, where one sample was excluded from the analyses because of low signal. A) The top 10 enriched transcription factor motifs under androgen deprivation associated with sites of AR and MED19 occupancy in MED19 LNCaP cells where AR is present only in MED19 LNCaP cells are shown, with ELK1 as the top associated transcription factor (labeled diagram of occupancy sites, right). B) ELK1 knockdown is the top hit from Transcription Factor Perturbation from Enrichr associated with genes upregulated by MED19 overexpression under androgen deprivation from the RNA-seq study; AR knockdown is also strongly associated. Fold downregulation of MAOA mRNA with associated ELK1 knockdown (GSE 34589) or associated AR knockdown (GSE 22483) is shown. C) ELK1 was depleted by siRNA and mRNA expression of MAOA in MED19 LNCaP cells cultured in androgen-depleted media was measured after 5 days (fold change expression normalized to RPL19, with MAOA mRNA expression with scrambled siRNA treatment set as "1"). Experiment was performed in biological triplicate, with representative results shown. D) ELK1 was depleted by siRNA and proliferation of MED19 LNCaP cells in androgen-depleted media was evaluated after 7 days, normalized to proliferation with scrambled siRNA (negative control, light grey). KIF11 knockdown is included as a positive control (black). Experiment was performed in biological duplicate, with representative results shown. E) Validation of ELK1 knockdown, with ELK1 mRNA measured as in C (with ELK1 mRNA expression with scrambled siRNA treatment set as "1"). F) ChIP-qPCR for ELK1 at the MAOA promoter overlapping with published ARE. $^{*}p < 0.05$; $^{**}p < 0.01$; and $^{***}p < 0.001$.

https://doi.org/10.1371/journal.pgen.1008540.g008

We next used Enrichr's "Transcription Factor Perturbation" tool to compare published gene expression changes with transcription factor knockdown or overexpression to our RNA-seq study. Strikingly, under androgen deprivation, genes upregulated with MED19

overexpression corresponded consistently to genes downregulated with ELK1 knockdown (top hit) or with AR knockdown, including MAOA (Figs 8B and S15B). However, with R1881 treatment, SP1 was not associated with genes upregulated with MED19 overexpression in the presence of androgens; rather, these were associated with SRF, which was not enriched in the ChIP-seq data (S15C Fig).

Given the strong connection to ELK1, we tested its functional role in gene expression and androgen-independent growth. We depleted ELK1 by siRNA in MED19 LNCaP cells and measured the effect on MAOA mRNA expression and proliferation under androgen deprivation. ELK1 knockdown both greatly reduced expression of MAOA and inhibited androgen-independent growth (Fig 8C–8E).

To determine if ELK1 occupied MAOA at sites where AR and MED19 were present, we performed ChIP-qPCR for ELK1 at the MAOA promoter region overlapping with the reported ARE, where AR, MED19, and H3K27 acetylation were present (Figs 8F and S17). Indeed, we found that ELK1 also occupied this region, with a trend toward increased ELK1 occupancy under androgen deprivation when MED19 is overexpressed (Fig 8F). This indicates that MED19 and ELK1 cooperate to enhance AR occupancy and H3K27 acetylation, increase MAOA expression, and promote androgen-independent growth.

Discussion

We have demonstrated that overexpression of MED19 in androgen-dependent LNCaP cells provides a growth advantage in the absence and presence of androgens. This is mediated by AR. The cells remain dependent on AR for growth under androgen deprivation, without increasing full-length AR abundance or splice variant AR-V7 expression. Therefore, increased expression of MED19 is sufficient to convert a cell that is androgen-dependent to one that is androgen-independent for growth.

Consistent with this are reports from our lab and others that MED19 depletion reduced AR transcriptional activity and growth of LNCaP cells and LNCaP-abl cells, which are derived from LNCaP cells and are androgen-independent [26,30]. We also reported that PC3 prostate cancer cells and HEK293 human embryonic kidney cells, both of which lack AR, were less sensitive to growth inhibition upon MED19 depletion compared to LNCaP-abl cells [26].

We expected that the selective effect by overexpressed MED19 on AR-associated gene expression, as well as genome-wide occupancy of MED19, AR, and H3K27 acetylation under androgen deprivation, would illuminate mechanism. Indeed, we observed by RNA-seq a defined set of genes that were differentially expressed upon MED19 overexpression in LNCaP cells compared to control cells. It should be noted that the changes in androgen-dependent gene expression reflect both primary and secondary effects of AR on gene expression, given that hormone treatment was done overnight. In addition, we observed a large overlap between MED19 and AR occupancy under both androgen-independent and androgen-dependent conditions. There was also a unique set of loci with AR and MED19 occupancy under androgen deprivation in MED19 LNCaP cells compared to control cells, suggesting that MED19 can drive AR to new sites. Thus, we observed upon MED19 overexpression a selective alteration of the AR cistrome. This was reflected in changes in gene expression under conditions of low androgen levels. This is likely via MED19 acting as part of the Mediator complex, and is consistent with the MED19 subunit being used to select the entire mammalian Mediator complex from mouse B cells for cryo-EM studies [27]. Although our previous report indicated that overexpressed AR co-immunoprecipitated with overexpressed FLAG-tagged MED19 in HEK293 cells, we did not find this to be the case for endogenous AR in MED19 LNCaP cells (S18 Fig) [26]. However, the Mediator subunit MED1 (another middle subunit) does co-

immunoprecipitate with FLAG-MED19, also consistent with MED19 acting as part of the Mediator complex (S18 Fig). The fact that MED1, which is well known to interact with AR, co-immunoprecipitates with MED19, suggests that MED19 could cooperate with AR via MED1 [46,47].

We also found that MAOA was upregulated upon MED19 overexpression in LNCaP cells under androgen deprivation. This was associated with an increase in occupancy of AR and H3K27 acetylation at the MAOA promoter. We also observed a striking growth-inhibitory effect upon MAOA depletion in MED19 LNCaP cells under androgen deprivation. Although MAOA is likely not the sole mediator of MED19-induced androgen-independent growth, it is important, given the large reduction in androgen-independent growth upon its depletion. Furthermore, multiple studies have established the importance of increased MAOA expression in facilitating prostate cancer proliferation [35,36,48,49]. Conversely, a polymorphism in the MAOA promoter conferring low expression is associated with lower risk of developing prostate cancer [50].

An ELK1 motif was enriched at sites occupied by AR, as well as MED19, in MED19 LNCaP cells but not in control LNCaP cells. Furthermore, MED19-upregulated genes, including MAOA, were associated with ELK1, suggesting that ELK1 could be cooperating with MED19 and AR to promote MAOA expression and growth under androgen deprivation. Indeed, MED19 overexpression promoted ELK1 occupancy at the MAOA promoter, and ELK1 depletion reduced MAOA expression and androgen-independent growth. ELK1 is an ETS transcription factor that controls AR transcriptional activity and promotes prostate cancer progression [20,23,24]. ELK1 has also been shown to interact directly with the AR ligand-independent N-terminal transcriptional activation domain [23,24]. Given the increase in H3K27 acetylation at the MAOA promoter with MED19 overexpression, it is possible that MED19, in conjunction with ELK1, could promote recruitment of HATs, such CBP and p300, which are also known AR co-regulators [10–12]. Consistent with this change in H3K27 acetylation, ELK1 has also been found to interact with CBP and p300 in other cell types [51,52].

Based on our findings, we propose a model whereby under conditions of androgen deprivation and MED19 upregulation, MED19-containing Mediator cooperates with ELK1 to recruit and stabilize AR, via its N-terminal domain, to the promoter of MAOA, and increases H3K27 acetylation at the MAOA promoter, through recruitment of HATs. Recruitment of Pol II ensues, upregulating MAOA and licensing cell growth under low androgen (Fig 9). Consistent with this model, the structural determination of the yeast Mediator complex by cryo-EM revealed MED19 contacts the carboxy terminal domain (CTD) tail of Pol II; these contacts between Mediator and the Pol II CTD serve to recruit and stabilize Pol II [53]. Recent structure determination of the mammalian Mediator complex confirmed the importance of the middle module—where MED19 resides—for CTD contact [27].

The Mediator subunit MED1 has been described to promote androgen-dependent AR activity through interaction with the ligand-binding domain of AR, and is overexpressed in prostate cancer [47,54–56]. It is possible that MED1 or other Mediator subunits play a role in MED19-induced androgen-independent growth. When each of the 33 subunits of Mediator is depleted under androgen deprivation from MED19 LNCaP cells and compared to androgen-independent LNCaP-abl cells, MED27, MED12, MED26 and to a lesser extent MED1, reduced proliferation of both MED19 LNCaP and LNCaP-abl cells, with an overall variable effect on growth from subunit-to-subunit (S19 Fig). We interpret this as multiple Mediator subunits being generally involved in regulating androgen-independent proliferation rather than exerting a MED19-specific effect.

Our study may also have implications for MED19 function in other cancers. For example, reduction of MED19 by siRNA has been reported to reduce the proliferation of certain breast,

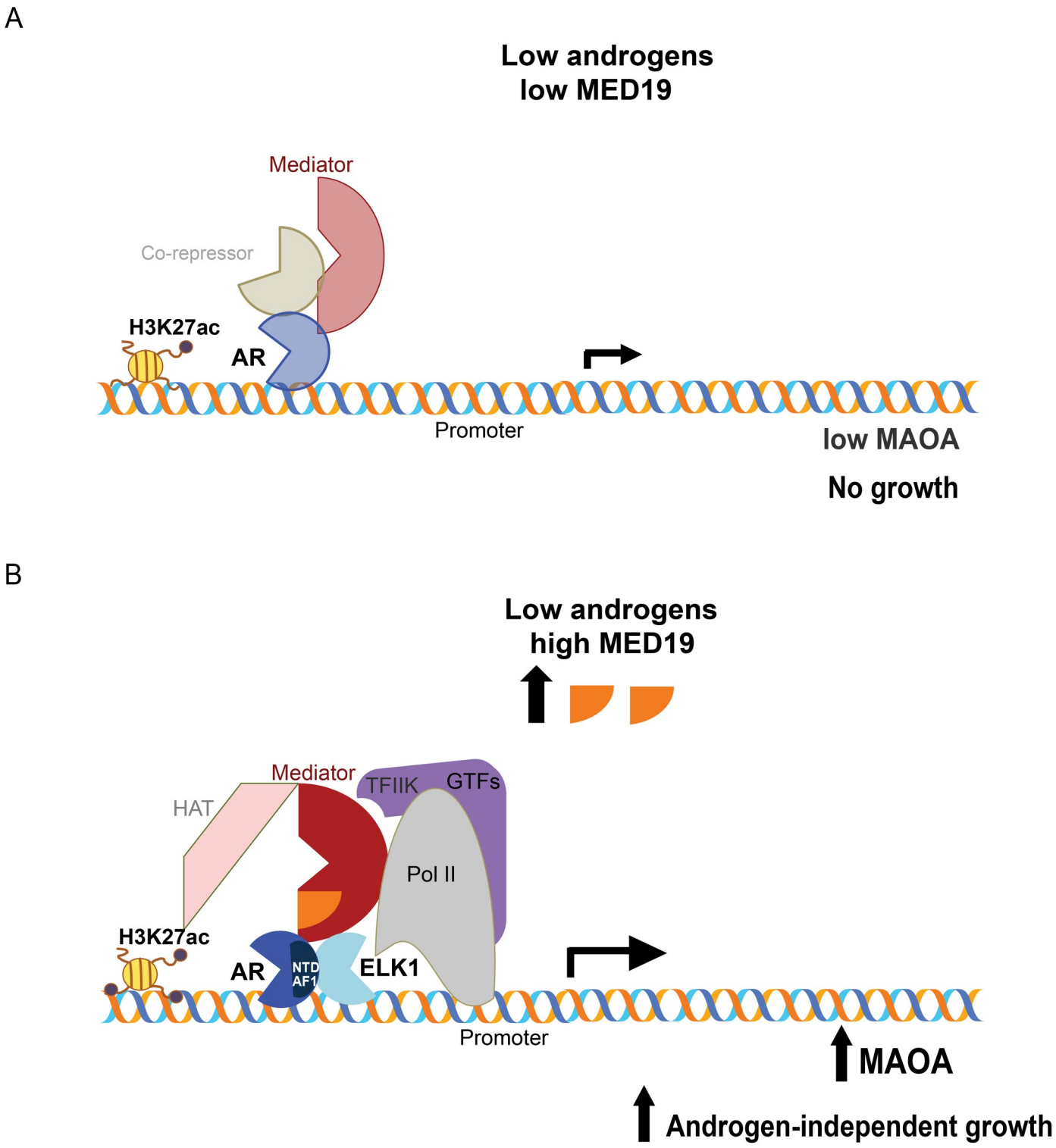

Fig 9. Model of MED19 driving androgen-independent growth by cooperating with ELK1 to promote AR occupancy and H3K27 acetylation at the MAOA promoter. A) Under low androgen and low MED19, AR occupancy is low at the MAOA promoter, MAOA is weakly expressed, and cells are growth-inhibited. B) When MED19 is upregulated, MED19 in Mediator cooperates with ELK1 to recruit and stabilize AR via its N-terminal domain (NTD) at the MAOA promoter, also recruiting Pol II and HATs, upregulating MAOA expression, and driving androgen-independent growth.

https://doi.org/10.1371/journal.pgen.1008540.g009

ovarian, cervical, and lung cancer cell lines, and increased abundance of MED19 protein is observed in tumors compared to benign tissue [21,57–63]. This suggests that MED19 functions with other transcription factors in other cell types to regulate gene expression and enhance cellular proliferation. Although the regulation of gene expression and cancer cell characteristics by Mediator subunits is complex, our study provides key insight into the mechanism of MED19 action in prostate cancer cells and androgen independence.

Materials and methods

Generation of LNCaP cells with stable overexpression of MED19

LNCaP cell lines purchased from the ATCC (Manassas, VA) were used for stable transfections. MED19 overexpression and empty vectors were purchased from Origene Technologies (NM_153450; plenti-myc-DDK-P2A-puro backbone). Cells were generated after lentiviral infection with the above constructs. Lentiviral particles were produced in the 293T/17 cell line (ATCC). LNCaP, RWPE-1, RWPE-2, and a mouse prostate stem cell (MSC) line expressing activated AKT were infected on two consecutive days with control or MED19 lentiviral particles and polybrene. Pooled clones were collected after selection with puromycin (1 μg/mL). MED19 expression was verified by western blot. Cells were routinely tested for mycoplasma, and only cells that were mycoplasma-free were used in the experiments.

Cell culture and reagents

LNCaP cell lines were maintained in complete RPMI: RPMI-1640 supplemented with 10% fetal bovine serum (FBS) (Hyclone; Fisher Scientific) and 1% penicillin-streptomycin (Cellgro; Mediatech, Inc.) For assays under androgen deprivation, cells were cultured in androgen-depleted RPMI: phenol red- and L-glutamine-free RPMI-1640 supplemented with 10% FBS dextran charcoal-stripped of androgens (c-FBS, Hyclone) and 1% L-glutamine (Cellgro Mediatech, Inc.). Cells were cultured on poly-d-lysine-coated plates. RWPE-1 cells and RWPE-2 cells were cultured in keratinocyte SFM media supplemented with L-glutamine, BPE, and EGF (Thermo Fisher Scientific) [31]. The mouse prostate stem cell line expressing activated AKT was cultured as described in [32]. R1881 (Perkin Elmer) was reconstituted in ethanol. Enzalutamide (MedKoo) was reconstituted in DMSO. Puromycin (Sigma Aldrich) was reconstituted in water.

Proliferation assay

Cells were plated in the appropriate media in quintuplicate (LNCaP: 3,000 cells per well in complete media and 5,000 cells per well in androgen-depleted media; RWPE-1: 2,000 cells per well; RWPE-2: 10,000 cells per well; mouse prostate stem cells: 1,000 cells per well) in poly-d-lysine-coated 96-well plates. Cell proliferation was determined using the Cyquant-NF Cell Proliferation Assay (Invitrogen) or PrestoBlue Cell Viability Assay (ThermoFisher Scientific). Fluorescence was quantified with the SpectraMaxM5 Microplate Reader and SoftMaxPro software (Molecular Devices) and normalized to readings at Day 0 (day after plating).

Colony formation assay

Cells were plated in the appropriate media in duplicate (LNCaP: 5,000 cells per well in complete media and 10,000 cells per well in androgen-depleted media in poly-d-lysine-coated 6-well plates for 10–14 days). Cells were fixed with 66% methanol/33% acetic acid solution and stained with 0.1% crystal violet solution.

Spheroid formation assay

Cells were plated in the appropriate media in 96-well ultra-low attachment plates (Corning) (LNCaP: 1,000–2,000 cells per well, 8 wells/condition) for 10–14 days. Cells were imaged with CellInsight CX7 LZR and spheroid area per well was analyzed by Cellomics Scan Version 6.6.1.

Xenograft study

For xenograft experiments, mouse prostate stem cells (5×10^6) were mixed with an equal volume of Matrigel and injected subcutaneously into the flank region of Nu/J (nude) male mice (Jackson Laboratories). Tumor volume was measured twice weekly. All animal studies were performed at NYU School of Medicine. The animal research was approved by the NYU School of Medicine Institutional Animal Care and Use Committee (IACUC), protocol number IA16-01775.

Immunohistochemistry

Immunohistochemistry (IHC) was performed on paraffin-embedded tissue sections that were dewaxed in xylene, rehydrated, and washed in phosphate-buffered saline (pH 7.4). Antigen retrieval was performed by heating sections in a microwave oven (900 watts) for 5 min in 10 mM citrate buffer, followed by treatment with 3% H_2O_2 and blocked with 20% normal goat serum. Sections at room temperature were incubated for 2 hours with antibody against phospho-AKT1 Ser473 (pAKT) (Cell Signaling Cat.#4060, 1:100 dilution), phospho-p44/p42 ERK1/2 (pERK) (Cell Signaling #4376, 1:500 dilution), Ki-67 (BD #550609, 1:50 dilution), and AR (AR N-20, Santa Cruz Biotech #sc-816, 1:500 dilution), washed, and followed by a 1 hour incubation with a biotinylated rabbit secondary (1:1000; Vector Labs). An avidin-biotin complex was formed and developed using diaminobenzidine chromagen, followed by a counterstain with hematoxylin.

RNA preparation and quantitative RT-PCR

Total RNA was extracted using RNeasy (Qiagen) according to the manufacturer's instructions. RNA (1 μg) was reverse transcribed using the Verso cDNA Synthesis Kit (ThermoFisher Scientific) following the manufacturer's instructions. Gene-specific cDNA was amplified in a 10-μL reaction containing Fast SYBR Green qPCR Master Mix (ThermoFisher Scientific). Real-time PCR was performed using the Applied Biosystems Quantstudio 6 Flex Real-Time PCR System with each gene tested in triplicate. Data were analyzed by the DDCT method using RPL19 as a control gene, and normalized to control samples, which were arbitrarily set to 1. The sequences of the primers used for real-time PCR are as follows.

RPL19 –F:CACAAGCTGAAGGCAGACAA, R:GCGTGCTTCCTTGGTCTTAG; ELK1 –F: CACATCATCTCCTGGACTTCAC, R:CGGCTGAGCTTGTCGTAAT; MED19 –F: CTGTGGCCCTTTTTACCTCA, R:GCTTCTCCTTCACCTTCTTCC;

AR–F:TACCAGCTCACCAAGCTCCT, R:GAACTGATGCAGCTCTCTCG; LRRTM3 –F: ATACGACCAGCCCACAATAAG, R: GCTCAGTCTCTAGGTGTGTTTC;

MAST4 –F:GCCAAAGAAGGACAGGGTATTA, R:GCTGTCCCACTATCGTAGTTTC;

MAOA–F:CCTGTGGTTCTTGTGGTATGT, R:CACCTACAAACTTCCGTTCCT; AR-V7 –F: CCATCTTGTCGTCTTCGGAAATGTTA, R: TTTGAATGAGGCAAGTCAGCCTTTCT;

FKBP5 –F:CGCAGGATATACGCCAACAT, R:CTTGCCCATTGCTTTATTGG;

PSA (KLK3)–F:CCAAGTTCATGCTGTGTGCT, R:GCACACCATTACAGACAAGTGG.

The RT2 Profiler PCR Array (PAHS-135) for androgen-dependent targets in prostate cancer profiled in S7 Fig were purchased from Qiagen.

siRNA knockdown

Three individual siRNAs (Silencer Select; Ambion, Life Technologies) were pooled and transfected into cells using the Lipofectamine RNAimax transfection reagent (ThermoFisher Scientific) following the manufacturer's instructions. Each siRNA sequence was cross-referenced with siRNA-Check to confirm specificity [64]. Scrambled non-targeting siRNA was used as the negative control for normalization in all knockdown experiments (specific design details proprietary to Ambion). We selected pooled siRNAs over individual siRNAs since it has been reported that siRNA pools show greater phenotypic penetrance than the individual duplexes [65]. siRNAs were used at a final concentration of 25 nM.

Protein extraction and western blot analysis

Cells were lysed in RIPA buffer supplemented with protease inhibitor cocktail (Cell Signaling Technology). Protein lysates were subjected to SDS/PAGE and immunoblotted with antibodies against AR (441, Santa Cruz Biotechnology; cat # sc-7305) or MYC tag (Cell Signaling Technology; cat # 2276S). Tubulin (Covance; cat # MMS-489P) was used as a loading control.

RNA-sequencing

RNA was prepared as described above. Libraries were prepared with ribodepletion using Illumina TruSeq stranded total RNA with RiboZero Gold library preparation kit. Sequencing was performed using the Illumina HiSeq2500 Sequencing system (HiSeq 4000 Paired-End 50 or PE75 Cycle Lane). Data was analyzed by Rosalind (https://rosalind.onramp.bio/), with a HyperScale architecture developed by OnRamp BioInformatics, Inc. (San Diego, CA). Reads were trimmed using cutadapt. Quality scores were assessed using FastQC. Reads were aligned to the Homo sapiens genome build hg19 using STAR. Individual sample reads were quantified using HTseq and normalized via Relative Log Expression (RLE) using DESeq2 R library. Read Distribution percentages, violin plots, identity heatmaps, and sample MDS plots were generated as part of the QC step using RSeQC. DEseq2 was also used to calculate fold changes and p-values. Clustering of genes for the final heatmap of differentially expressed genes was done using the PAM (Partitioning Around Medoids) method using the fpc R library. Functional enrichment analysis of pathways, gene ontology, domain structure and other ontologies was performed using HOMER. Several database sources were referenced for enrichment analysis, including Interpro, NCBI, MSigDB REACTOME, WikiPathways. Enrichment was calculated relative to a set of background genes relevant for the experiment. Additional gene enrichment is available from the following partner institutions: Advaita (http://www.advaitabio.com/ipathwayguide). Differentially expressed genes were also analyzed using the Enrichr platform from the Ma'ayan Laboratory, including ChEA and "Transcription Factor (TF) Perturbations Followed by Expression" analyses [66,67].

Chromatin immunoprecipitation (ChIP)-sequencing

Cells were double crosslinked with formaldehyde and the bifunctional protein crosslinker disuccinimidyl glutarate (DSG) to preserve both protein-DNA and protein-protein interactions.

A mixture of two antibodies for AR ChIP was used, one against the C-terminus and one against the N-terminus, to maximize AR enrichment and minimize epitope masking. Antibodies were tested and optimized. The ChIP-seq study was performed in independent biological triplicates (one sample for ChIP-seq for AR in control LNCaP cells + R1881 was excluded from the analyses because of low signal). Inputs were used for normalization and additional IgG controls included to ensure any low occupancy peaks were specific to AR and not background. We discarded any peaks for AR and for H3K27 acetylation that scored above 0 for IgG; this was also done with peaks for FLAG-MED19 in MED19 LNCaP cells that scored above 0 for FLAG in control LNCaP cells (very few peaks scored above 0 and overlapped in either case) (S8C Fig and S7 Table). Rigorous scoring of peaks was done using the Rosalind platform (see below).

Protocol for ChIP-seq was adapted from Fonseca *et al* [68]. Briefly, cells were double cross-linked with DSG (ProteoChem; cat # c1104) for 20 min and 1% formaldehyde for 10 min. Crosslinking was quenched with Tris-HCl pH 7.5. Cells were collected, washed with PBS, and cell pellets snap frozen with liquid nitrogen. Cell pellets were resuspended in nuclei isolation buffer (50 mM Tris–pH 8.0, 60 mM KCl, 0.5% NP40), nuclei collected, and resuspended in sonication buffer (RIPA buffer). Samples were sonicated in TPX PMP tubes (Diagenode) for 60 min (30 sec. on, 30 sec. off) in a Bioruptor sonicator (Diagenode). Inputs (10%) were collected and supernatants were then incubated overnight with the following antibodies pre-incubated with Protein A and Protein G Dynabeads (Invitrogen): a mixture of AR antibodies (AR 441 mouse monoclonal, Santa Cruz Biotechnology, cat # sc-7305) and (AR D6F11 rabbit monoclonal, Cell Signaling Technology, cat # 5153); DYKDDDDK Tag (FLAG epitope) (Cell Signaling Technology, cat # 14793); or acetylated H3K27 (Active Motif, cat # 39034). Control ChIPs were performed with normal mouse IgG (Santa Cruz Biotechnology, cat # sc-2025) and normal rabbit IgG (Sigma Aldrich, cat # 12–370). Immunocomplexes were then washed and cross-linking reversed overnight at 65˚C with 5 M NaCl. DNA was isolated with the Zymo Chip DNA Clean and Concentrator kit (Zymo Research). Libraries were prepared according to the protocol described in [68]. Sequencing was performed using Illumina HiSeq4000 Sequencing (HiSeq 4000 Single Read 50 Cycle Lane).

Data were analyzed by Rosalind (https://rosalind.onramp.bio/), with a HyperScale architecture developed by OnRamp BioInformatics, Inc. (San Diego, CA). Reads were trimmed using cutadapt. Quality scores were assessed using FastQC. Reads were aligned to the Homo sapiens genome build hg19 using bowtie2. Per-sample quality assessment plots were generated with HOMER and Mosaics. Peaks were called using MACS2 (with input controls background subtracted). Peak overlaps were analyzed using the DiffBind R library. Read distribution percentages, identity heatmaps, and FRiP plots were generated as part of the QC step using ChIPQC R library and HOMER. HOMER was also used to generate known and de novo motifs and perform functional enrichment analysis of pathways, gene ontology, domain structure and other ontologies.

ChIP-qPCR

ChIPs were performed as described above, with ChIPs for AR, FLAG epitope, acetylated H3K27, and ELK1 (abcam, cat # ab32106). IgGs were included as negative controls. After DNA isolation, qPCR was performed as described above, with primers targeting the MAOA promoter region—F: TGTCAAGGCAGGCGTCTAC, R: GGACCCTTGTACTGACAC. Relative enrichment was calculated as a percentage of 10% input.

Statistical analyses

Statistical analyses were performed using GraphPad Prism software. Data are reported as mean ± SEM (technical replicates for each experiment described above). Number of

experiments are described in the figure legends; unless otherwise noted, two-tailed unpaired Student's t test was used when comparing two groups, with a p value < 0.05 being considered significant and levels of significance denoted as $^{*}p < 0.05$; $^{**}p < 0.01$; and $^{***}p < 0.001$.

Supporting information

S1 Fig. MED19 LNCaP cells stably overexpress MED19. MED19 LNCaP cells with stable overexpression of MYC- and FLAG-tagged MED19 and control LNCaP cells with stable expression of the empty vector were created by lentiviral transduction, with pooled clones selected with puromycin. After selection, stable overexpression of MED19 in MED19 LNCaP cells was confirmed. A) Scheme of the lentiviral expression construct MED19 (NM_153450) (adapted from Origene). B) RNA was extracted and qPCR was performed for MED19 in control LNCaP cells and MED19 LNCaP cells to confirm upregulation of MED19 mRNA (fold change expression normalized to RPL19 with MED19 mRNA expression in control LNCaP cells set as "1"). $^{***}p < 0.001$. C) MED19 LNCaP cells and control LNCaP cells were treated with MED19 siRNA or scrambled siRNA, and total protein lysates were probed by MYC tag. Tubulin was used as a loading control. D) Validation of MED19 knockdown, with MED19 mRNA measured as in B (with MED19 mRNA expression with scrambled siRNA treatment set as "1").
(PDF)

S2 Fig. Expression, morphology, and protein abundance of MED19 in control LNCaP cells and MED19 LNCaP cells. A) Control LNCaP and MED19 LNCaP cells were cultured in complete media, fixed with paraformaldehyde, permeabilized, and stained with a mouse monoclonal antibody to MYC (Myc-Tag (9B11) Cell Signaling #2276), which is an epitope tag on the MED19 expression construct (see S1A Fig), followed by a secondary antibody (Texas Red anti-mouse), along with DAPI to identify the nucleus (blue), with fluorescent images captured using EVOS Cell Imaging System. Shown is 20X magnification. B) Morphology of control LNCaP and MED19 LNCaP cells. Cells were cultured in androgen-containing media and in androgen-depleted media for 3 days, and imaging of live cells was performed using the EVOS Cell Imaging System. Shown are 20X images. C) Western blot of MED19 from control LNCaP and MED19 LNCaP cells using an antibody to MED19 (developed in our laboratory) that recognizes the endogenous and overexpressed MED19. Tubulin serves as a loading control.
(PDF)

S3 Fig. MED19 RWPE-1 cells have comparable MED19 expression to MED19 RWPE-2 cells. Total protein lysates from RWPE-1 and RWPE-2 cells stably expressing FLAG- and MYC-tagged MED19 (MED19 RWPE-1 and MED19 RWPE-2) or empty vector (control RWPE-1 and control RWPE-2) were probed for MYC tag, with tubulin used as a loading control.
(PDF)

S4 Fig. Potential activation of ERK and AR in tumors from MED19 MSC. Immunohistochemistry of formalin-fixed, paraffin-embedded tissue sections from control MSC and MED19 MSC using antibodies against A) phospho-AKT1 Ser473 (pAKT) (Cell Signaling Cat. #4060, 1:100 dilution), B) phospho-p44/p42 ERK1/2 (pERK) (Cell Signaling Cat. #4376, 1:500 dilution), C) Ki-67 (BD Cat. #550609, 1:50 dilution), and D) AR (AR N-20, Santa Cruz Cat. #sc-816, 1:500 dilution). White arrow shows a cluster of cells with strong pERK staining in a tissue section from a MED19 MSC tumor.
(PDF)

S5 Fig. MED19 LNCaP cells do not express AR-V7. MED19 LNCaP cells and control LNCaP cells were cultured under androgen deprivation for 3 days and treated overnight with ethanol vehicle. RNA was extracted and mRNA measured by qPCR for AR-V7 mRNA (fold change expression normalized to RPL19 with AR-V7 mRNA expression in control LNCaP cells set as "1"). LNCaP-95 cells that express AR-V7 were used as a positive control. $^{*}p < 0.05$; $^{**}p < 0.01$; and $^{***}p < 0.001$. ns = not significant.
(PDF)

S6 Fig. MED19 LNCaP cells are sensitive to AR knockdown. MED19 LNCaP cells were cultured in A) androgen-depleted media or B) androgen-containing media, with control LNCaP cells. AR was depleted by siRNA and proliferation was evaluated after 7 days, normalized to proliferation with scrambled siRNA. KIF11 was used as a positive control. Experiment was performed in biological duplicate, with representative results shown. $^{*}p < 0.05$; $^{**}p < 0.01$; and $^{***}p < 0.001$. ns = not significant. C) Validation of AR knockdown (fold change expression normalized to RPL19 and AR mRNA expression with scrambled siRNA treatment set as "1").
(PDF)

S7 Fig. MED19 selectively regulates specific AR target genes. MED19 LNCaP cells and control LNCaP cells were cultured under androgen deprivation for 3 days and treated for 16 h with ethanol vehicle or 10 nM R1881. RNA was extracted and mRNA measured by qPCR for the AR target genes indicated (fold change expression normalized to RPL19 with target gene mRNA expression in vehicle-treated control LNCaP cells set as "1"). Experiment was performed in biological triplicate, with representative results shown. $^{*}p < 0.05$; $^{**}p < 0.01$; and $^{***}p < 0.001$. ns = not significant.
(PDF)

S8 Fig. QC of ChIP-seq samples. MED19 LNCaP cells and control LNCaP cells were cultured under androgen deprivation for 3 days and treated with ethanol vehicle or 100 nM R1881 for 4 h. ChIP-seq for FLAG-MED19, AR, and H3K27ac was performed in biological triplicate with the exception of ChIP-seq for AR in control LNCaP cells + R1881, where one sample was excluded from the analyses because of low signal. A) ChIP-qPCR QC of AR, H3K27ac, and FLAG-MED19 ChIPs are shown, with normalization to inputs. AR occupancy and H3K27ac at PSA ARE III greatly increase in response to R1881 treatment. IgG is shown as a negative control. FLAG-MED19 shows high occupancy in MED19 LNCaP cells at PDZK1P1, identified as a site of strong FLAG-MED19 occupancy from a pilot ChIP-seq for FLAG-MED19. FLAG in control LNCaP cells is shown as a negative control. Experiments were performed in biological triplicate, with representative results shown. $^{*}p < 0.05$; $^{**}p < 0.01$; and $^{***}p < 0.001$. B) ChIP-seq tracks (representative results) for AR and H3K27ac at PSA and FKBP5 in control LNCaP cells with vehicle or R1881 treatment. AR occupancy and H3K27ac clearly increase in response to R1881 treatment (occupancy scores in S7 Table). C) Overlap of IgG with AR (left) and H3K27ac sites (middle); and overlap of FLAG in control LNCaP cells with FLAG-MED19 in MED19 LNCaP cells (right). All normalized to input. IgG and FLAG-control yield very few sites, with minimal overlap (all sites in S7 Table).
(PDF)

S9 Fig. QC and qPCR validation of RNA-seq. MED19 LNCaP cells and control LNCaP cells were cultured under androgen deprivation for 3 days and treated for 16 h with ethanol vehicle or 10 nM R1881. RNA-seq was performed in biological triplicate. Graphs represent fold changes from qPCR (fold change expression normalized to RPL19 with PSA or FKBP5 mRNA expression in vehicle-treated cells set as "1") and tables represent fold changes from RNA-seq.

Upregulation of PSA and FKBP5 mRNA expression in A) control LNCaP cells and B) MED19 LNCaP cells in response to R1881 treatment, with consistency between RNA-seq and qPCR, and expected increase in expression with R1881 treatment. Experiments were performed in biological triplicate, with representative results shown. $^{*}p < 0.05$; $^{**}p < 0.01$; and $^{***}p < 0.001$.
(PDF)

S10 Fig. Binding site heatmaps for AR occupancy, FLAG-MED19 occupancy, and H3K27 acetylation. Control LNCaP and MED19 LNCaP cells were cultured under androgen deprivation for 3 days and treated with ethanol vehicle or 100 nM R1881 for 4 hours. ChIP-seq for FLAG-MED19, AR, and H3K27ac were performed and in biological triplicate, with the exception of ChIP-seq for AR in control LNCaP cells + R1881, where one sample was excluded from the analyses because of low signal. A) Binding heatmaps for AR occupancy in control LNCaP and MED19 LNCaP cells. Brown = sites occupied by AR in both control LNCaP and MED19 LNCaP cells; blue = sites occupied by AR in control LNCaP cells only; orange = sites occupied by AR in MED19 LNCaP cells only. B) Binding heatmaps for H3K27 acetylation. Brown = sites of H3K27 acetylation in both control LNCaP and MED19 LNCaP cells; blue = sites of H3K27 acetylation in control LNCaP cells only; orange = sites of H3K27 acetylation in MED19 LNCaP cells only. C) Binding heatmaps for AR and FLAG-MED19 in MED19 LNCaP cells. Brown = sites occupied by AR and FLAG-MED19; blue = sites occupied by AR only; orange = sites occupied by FLAG-MED19 only. D) Binding heatmaps for AR, FLAG-MED19, and H3K27ac in MED19 LNCaP cells. Dark brown-green = sites occupied by AR and FLAG-MED19 and marked by H3K27 acetylation; medium green = sites occupied by AR and marked by H3K27 acetylation; medium brown-green = sites of FLAG-MED19 occupancy and marked by H3K27 acetylation; brown = sites of AR and FLAG-MED19 occupancy; light green = sites of H3K27 acetylation only; blue = sites occupied by AR only; orange = sites occupied by FLAG-MED19 only.
(PDF)

S11 Fig. MED19 alters mRNA expression, AR occupancy, and H3K27 acetylation for LRRTM3 without or with androgens, but LRRTM3 does not affect androgen-independent growth. MED19 LNCaP cells and control LNCaP cells were cultured under androgen deprivation for 3 days and treated with ethanol vehicle or R1881 (10 nM 16 hours for RNA-seq; 100 nM 4 hours for ChIP-seq). RNA-seq and ChIP-seq for FLAG-MED19, AR, and H3K27ac were performed in biological triplicate, with the exception of ChIP-seq for AR in control LNCaP cells + R1881, where one sample was excluded from the analyses because of low signal. A) Fold change mRNA expression from RNA-seq and qPCR validation of changes in LRRTM3 mRNA expression (performed in biological triplicate, representative results shown; fold change expression normalized to RPL19 with LRRTM3 mRNA expression in vehicle-treated control LNCaP cells set as "1"). Greater fold changes by qPCR likely due to low abundance (raw counts in RNA-seq) of LRRTM3 in control LNCaP cells. B) ChIP-seq tracks (representative results) for FLAG-MED19, AR, and H3K27ac for androgen deprivation or R1881 treatment are shown for intronic regions of LRRTM3. Fold change (up (+) or down (-)) in occupancy scores for MED19 LNCaP cells compared to control LNCaP cells shown for each peak (see S6 Table for all occupancy scores). ++ indicates positive occupancy score in MED19 LNCaP cells and a score of zero in control LNCaP cells;—indicates an occupancy score of zero in MED19 LNCaP cells and a positive score in control LNCaP cells. C) LRRTM3 was depleted by siRNA and proliferation of MED19 LNCaP cells in androgen-depleted media was evaluated after 7 days, normalized to proliferation with scrambled siRNA (negative control, light grey). KIF11 knockdown is included as a positive control (black). Experiment was performed in biological

duplicate, with representative results shown. $^{*}p < 0.05$; $^{**}p < 0.01$; and $^{***}p < 0.001$.
(PDF)

S12 Fig. MED19 alters mRNA expression, AR occupancy, and H3K27 acetylation for MAST4. MED19 LNCaP cells and control LNCaP cells were cultured under androgen deprivation for 3 days and treated with ethanol vehicle or R1881 (10 nM 16 hours for RNA-seq; 100 nM 4 hours for ChIP-seq). RNA-seq and ChIP-seq for FLAG-MED19, AR, and H3K27ac were performed and in biological triplicate, with the exception of ChIP-seq for AR in control LNCaP cells + R1881, where one sample was excluded from the analyses because of low signal. A) Fold change mRNA expression from RNA-seq and qPCR validation of changes in MAST4 mRNA expression (performed in biological triplicate, representative results shown; fold change expression normalized to RPL19 with MAST4 mRNA expression in vehicle-treated control LNCaP cells set as "1"). $^{*}p < 0.05$; $^{**}p < 0.01$; and $^{***}p < 0.001$. B) ChIP-seq tracks (representative results) for FLAG-MED19, AR, and H3K27ac for androgen deprivation or R1881 treatment are shown for promoter and intronic regions of MAST4. Fold change (up (+) or down (-)) in occupancy scores for MED19 LNCaP cells compared to control LNCaP cells shown for each peak (see S6 Table for all occupancy scores). ++ indicates positive occupancy score in MED19 LNCaP cells and a score of zero in control LNCaP cells;—indicates an occupancy score of zero in MED19 LNCaP cells and a positive score in control LNCaP cells.
(PDF)

S13 Fig. MED19 and androgen treatment promote mRNA expression, AR occupancy, and H3K27 acetylation for MAOA. MED19 LNCaP cells and control LNCaP cells were cultured under androgen deprivation for 3 days and treated with ethanol vehicle or R1881 (10 nM 16 hours for RNA-seq; 100 nM 4 hours for ChIP-seq). RNA-seq and ChIP-seq for FLAG-MED19, AR, and H3K27ac were performed in biological triplicate, with the exception of ChIP-seq for AR in control LNCaP cells + R1881, where one sample was excluded from the analyses because of low signal. A) Fold change mRNA expression from RNA-seq and qPCR validation of changes in MAOA mRNA expression (performed in biological triplicate, representative results shown; fold change expression normalized to RPL19 with MAOA mRNA expression in vehicle-treated control LNCaP cells set as "1"). B) ChIP-seq tracks (representative results) for FLAG-MED19, AR, and H3K27ac for androgen deprivation or R1881 treatment are shown for the promoter region of MAOA. Fold change (up (+) or down (-)) in occupancy scores for MED19 LNCaP cells compared to control LNCaP cells shown for each peak (see S6 Table for all occupancy scores). ++ indicates positive occupancy score in MED19 LNCaP cells and a score of zero in control LNCaP cells;—indicates an occupancy score of zero in MED19 LNCaP cells and a positive score in control LNCaP cells. C) ChIP-qPCR for FLAG-MED19, AR, and H3K27ac at the MAOA promoter overlapping with published ARE. (Control–control LNCaP cells; MED19 –MED19 LNCaP cells; veh–vehicle treatment; R1881 –R1881 treatment). Experiment was performed in biological duplicate, with representative results shown. $^{*}p < 0.05$; $^{**}p < 0.01$; and $^{***}p < 0.001$. ns = not significant.
(PDF)

S14 Fig. FOXA1 and FOXM1 are enriched at sites of AR occupancy and MED19 occupancy in the absence and presence of androgens. MED19 LNCaP cells and control LNCaP cells were cultured under androgen deprivation for 3 days and treated with ethanol vehicle or 100 nM R1881 for 4 hours. ChIP-seq for FLAG-MED19, AR, and H3K27ac was performed in biological triplicate, with the exception of ChIP-seq for AR in control LNCaP cells + R1881, where one sample was excluded from the analyses because of low signal. A) Top 10 enriched transcription factor motifs under androgen deprivation, associated with MED19 sites in

MED19 LNCaP cells (top), MED19 and AR occupied sites in MED19 LNCaP cells (middle top), AR sites in MED19 LNCaP cells (middle bottom), and AR sites in control LNCaP cells (bottom). B) Top 10 enriched transcription factor motifs with R1881 treatment, associated with MED19 sites in MED19 LNCaP cells (top), MED19 and AR occupied sites in MED19 LNCaP cells (middle top), AR sites in MED19 LNCaP cells (middle bottom), and AR sites in control LNCaP cells (bottom).
(PDF)

S15 Fig. Enriched ChIP-seq motifs unique to AR+MED19 in MED19 LNCaP cells with R1881 treatment and gene changes associated with Enrichr Transcription Factor Perturbation with vehicle or R1881 treatment. A) Top 10 enriched transcription factor motifs with R1881 treatment associated with sites of AR and MED19 occupancy in MED19 LNCaP cells where AR is present only in MED19 LNCaP cells, with SP1 as the top associated transcription factor. B) Gene changes associated with ELK1 knockdown and AR knockdown from Enrichr Transcription Factor Perturbation, compared to MED19 overexpression under androgen deprivation from the RNA-seq study. C) SRF knockdown is the top hit from Enrichr Transcription Factor Perturbation, associated with genes upregulated by MED19 overexpression with R1881 treatment from the RNA-seq study (top); corresponding genes changes associated with SRF knockdown compared to MED19 overexpression (bottom).
(PDF)

S16 Fig. FOXA1 and FOXM1 and AR-related motifs are enriched at sites of AR and MED19 occupancy with R1881 treatment. MED19 LNCaP cells and control LNCaP cells were cultured under androgen deprivation for 3 days and treated with ethanol vehicle or 100 nM R1881 for 4 hours. ChIP-seq for FLAG-MED19, AR, and H3K27ac was performed in biological triplicate, with the exception of ChIP-seq for AR in control LNCaP cells + R1881, where one sample was excluded from the analyses because of low signal. A) Top 10 enriched transcription factor motifs associated with AR sites in control LNCaP cells for R1881 vs. vehicle treatment, with enrichment of AR-related motifs in response to R1881 treatment. B) Top 10 enriched transcription factor motifs associated with AR sites in MED19 LNCaP cells for R1881 vs. vehicle treatment, with enrichment of AR-related motifs in response to R1881 treatment. C) Top 10 enriched transcription factor motifs associated with MED19 sites in MED19 LNCaP cells for R1881 vs. vehicle treatment, with enrichment of AR-related motifs in response to R1881 treatment.
(PDF)

S17 Fig. QC of ELK1 ChIP. MED19 LNCaP cells and control LNCaP cells were cultured under androgen deprivation for 3 days and treated with ethanol vehicle or 100 nM R1881 for 4 hours, and ChIP-qPCR for ELK1 was performed. ELK1 occupancy at previously published ELK1 sites was verified in control LNCaP cells (top) and MED19 LNCaP cells (bottom), with occupancy verified +/- R1881 for sites at A) Chr.1 and B) Chr. 6. Normalization to inputs was done and IgG is shown as a negative control. $^{*}p < 0.05$; $^{**}p < 0.01$; and $^{***}p < 0.001$. ns = not significant.
(PDF)

S18 Fig. MED1 but not AR co-immunoprecipitates with overexpressed MED19. MED19 LNCaP and control LNCaP cells were cultured in androgen-containing media. Cells were lysed with RIPA buffer, input was collected, and FLAG-tagged MED19 was immunoprecipitated using FLAG antibody coupled to protein A/G agarose beads. Total protein lysates (input), FLAG immunoprecipitates, and flow through were collected and probed with antibodies for MYC (for overexpressed MED19), AR, and MED1. Tubulin was used as a loading

control for input. Experiment was performed in biological duplicate, with representative results shown.
(PDF)

S19 Fig. Depletion of Mediator subunits in MED19 LNCaP cells and LNCaP-abl cells under androgen deprivation. Each Mediator subunit or associated factor from the kinase module was depleted by siRNA and proliferation in androgen-depleted media was evaluated after 5 days, normalized to proliferation with scrambled siRNA (negative control, light grey). KIF11 knockdown is included as a positive control (black). MED19 depletion is highlighted in bold. A) Knockdown of Mediator subunits in MED19 LNCaP cells. B) Knockdown of Mediator subunits in LNCaP-abl cells. $^{*}p < 0.05$; $^{**}p < 0.01$; and $^{***}p < 0.001$. ns = not significant. Statistics denote comparison to scrambled siRNA. There is no statistically significant difference in growth between MED19 depletion and MED1 depletion in MED19 LNCaP cells or in LNCaP-abl cells. There is no statistically significant difference in growth between MED19 depletion and MED26/MED4/MED18/CDK19/MED12/MED27 depletion in MED19 LNCaP cells.
(PDF)

S20 Fig. Full western blot for MED19 LNCaP cell stable overexpression of MED19 protein from S1 Fig. A) Full western blot from S1 Fig. B) Membrane overlay of full western blot from S1 Fig.
(PDF)

S1 Table. Full list of 151 genes from RNA-seq significantly altered ≥1.5-fold (p-adj≤0.05) in MED19 LNCaP cells compared to control LNCaP cells, cultured under androgen deprivation for 3 days and treated overnight (16 h) with ethanol vehicle. 76 genes are upregulated (including MED19, top) and 75 genes are downregulated. P-values, p-adjusted values, fold changes, and gene descriptions are shown for each gene (sheet 1). Genes responsive to R1881 treatment from the RNA-seq (sheet 2), AR targets from ChEA (sheet 3), and androgen-responsive or AR targets from the literature (sheet 4) are shown.
(XLSX)

S2 Table. Full list of 309 genes from RNA-seq significantly altered ≥1.5-fold (p-adj≤0.05) in MED19 LNCaP cells compared to control LNCaP cells, cultured under androgen deprivation for 3 days and treated overnight (16 h) with 10 nM R1881. 78 genes are upregulated (including MED19, top) and 231 genes are downregulated. P-values, p-adjusted values, fold changes, and gene descriptions are shown for each gene (sheet 1). Genes responsive to R1881 treatment from the RNA-seq (sheet 2), AR targets from ChEA (sheet 3), and androgen-responsive or AR targets from the literature (sheet 4), are shown.
(XLSX)

S3 Table. Full list of 4430 genes from RNA-seq significantly altered ≥1.5-fold (p-adj≤0.05) in control LNCaP cells treated overnight (16 h) with 10 nM R1881 compared to control LNCaP cells treated overnight (16 h) with ethanol vehicle, under androgen deprivation for 3 days. 2361 genes are upregulated and 2069 genes are downregulated. P-values, p-adjusted values, fold changes, and gene descriptions are shown for each gene.
(XLSX)

S4 Table. Full list of 5041 genes from RNA-seq significantly altered ≥1.5-fold (p-adj≤0.05) in MED19 LNCaP cells treated overnight (16 h) with 10 nM R1881 compared to MED19 LNCaP cells treated overnight (16 h) with ethanol vehicle, under androgen deprivation for 3 days. 2727 genes are upregulated and 2314 genes are downregulated. P-values, p-

adjusted values, fold changes, and gene descriptions are shown for each gene.
(XLSX)

S5 Table. Response of MED19 LNCaP cells vs. control LNCaP cells to androgens. Top 100 androgen-induced (sheet 1) and androgen-repressed (sheet 2) genes for control LNCaP cells and MED19 LNCaP cells, with fold changes for each shown in comparison. Genes with 1.5-fold or more change in mRNA expression in response to androgen only in control LNCaP cells (sheet 3) or only in MED19 LNCaP cells (sheet 4).
(XLSX)

S6 Table. FLAG-MED19, AR, and H3K27ac occupancy in MED19 LNCaP cells at genes differentially expressed with MED19 overexpression in the absence and presence of androgens. Occupancy shown for androgen deprivation (sheet 1) and with R1881 treatment (sheet 2), with fold change in expression upon MED19 overexpression indicated. Androgen responsiveness of each gene in control LNCaP cells and MED19 LNCaP cells is also indicated. AR occupancy scores for LRRTM3 (sheet 3), MAST4 (sheet 4), and MAOA (sheet 5).
(XLSX)

S7 Table. AR occupancy score QC and background peaks. AR occupancy scores for PSA and FKBP5 (sheet 1); and list of background peaks for IgG (sheet 2) and FLAG in control LNCaP cells (sheet 3) for ChIP-seq.
(XLSX)

Acknowledgments

We thank Dr. Chi Yun, Dr. Sokha Nhek, Rebecca Lee, Dr. David Kahler, and the NYU High Throughput Biology Laboratory for technical support and advice. We thank Dr. Adriana Heguy, Paul Zappile, and the Genome Technology Center for technical support. We thank Drs. Christopher Glass, Gregory Fonseca, and Jenhan Tao for reagents, protocols, and technical assistance with the ChIP-seq studies. We thank Dr. Elaine Wilson for the AKT-transformed mouse prostate stem cell line. We thank Dr. Gregory David and Susan Ha for critical insight and assessment of the manuscript, and the Garabedian and Logan laboratories for their support.

Author Contributions

Conceptualization: Hannah Weber, Michael J. Garabedian.

Data curation: Hannah Weber, Rachel Ruoff.

Formal analysis: Hannah Weber, Rachel Ruoff, Michael J. Garabedian.

Funding acquisition: Michael J. Garabedian.

Investigation: Hannah Weber, Rachel Ruoff.

Project administration: Michael J. Garabedian.

Supervision: Michael J. Garabedian.

Validation: Hannah Weber, Rachel Ruoff.

Visualization: Hannah Weber, Rachel Ruoff.

Writing – original draft: Hannah Weber.

Writing – review & editing: Hannah Weber, Rachel Ruoff, Michael J. Garabedian.

References

1. Chan S, Dehm S. Constitutive activity of the androgen receptor. Advances in Pharmacology. 2014; 70:327–66.
2. Claessens F, Helsen C, Prekovic S, Broeck TVd, Spans L, Poppel HV, et al. Emerging mechanisms of enzalutamide resistance in prostate cancer. Nat Rev Urol. 2014; 11:712–16.
3. Harris W, Mostaghel E, Nelson P, Montgomery B. Androgen deprivation therapy: progress in understanding mechanisms of resistance and optimizing androgen depletion. Nature Clinical Practice Urology. 2009; 6:76–85.
4. Shen M, Abate-Shen C. Molecular genetics of prostate cancer: new prospects for old challenges. Genes Dev. 2010; 24:1967–2000.
5. Watson P, Arora V, Sawyers C. Emerging mechanisms of resistance to androgen receptor inhibitors in prostate cancer. Nature Reviews Cancer. 2015; 15:701–11.
6. Chandrasekar T, Yang J, Gao A, Evans C. Mechanisms of resistance in castration-resistant prostate cancer (CRPC). Translational Andrology and Urology. 2015; 4:365–80.
7. Labbe D, Brown M. Transcriptional Regulation in Prostate Cancer. Cold Spring Harbor Perspectives in Medicine. 2018; 8:a030437.
8. Dai C, Heemrs H, Sharifi N. Androgen Signaling in Prostate Cancer. Cold Spring Harbor Perspectives in Medicine. 2017; 7:a030452.
9. Heemers H, Tindall D. Androgen Receptor (AR) Coregulators: A Diversity of Functions Converging on and Regulating the AR Transcriptional Complex. Endocr Rev. 2007; 28:778–808.
10. Debes J, Sebo T, Lohse C, Murphy L, Haugen D, Tindall D. p300 in prostate cancer proliferation and progression. Cancer Research. 2003; 63:7638–40.
11. Fu M, Wang C, Reutens A, Wang J, Angeletti R, Siconolfi-Baez L, et al. p300 and p300/cAMP-response element-binding protein-associated factor acetylate the androgen receptor at sites governing hormone-dependent transactivation. Journal of Biological Chemistry. 2000; 275:20853–60.
12. Ianculescu I, Wu D, Siegmund K, Stallcup M. Selective roles for cAMP response element-binding protein binding protein and p300 protein as coregulators for androgen-regulated gene expression in advanced prostate cancer cells. Journal of Biological Chemistry. 2012; 287:4000–13.
13. Jin L, Garcia J, Chan E, Cruz Cdl, Segal E, Merchant M, et al. Therapeutic Targeting of the CBP/p300 Bromodomain Blocks the Growth of Castration-Resistant Prostate Cancer. Cancer Research. 2017; 77:5564–75.
14. Urbanucci A, Barfeld S, Kytölä V, Itkonen H, Coleman I, Vodák D, et al. Androgen Receptor Deregulation Drives Bromodomain-Mediated Chromatin Alterations in Prostate Cancer. Cell Reports. 2017; 19:2045–59.
15. Cai L, Tsai Y, Wang P, Wang J, Li D, Fan H, et al. ZFX Mediates Non-canonical Oncogenic Functions of the Androgen Receptor Splice Variant 7 in Castrate-Resistant Prostate Cancer. Molecular Cell. 2018; 72:341–54.
16. Asangani I, Dommeti V, Wang X, Malik R, Cieslik M, Yang R, et al. Therapeutic targeting of BET bromodomain proteins in castration-resistant prostate cancer. Nature. 2014; 510:278–82.
17. Piha-Paul S, Sachdev J, Barve M, PLoRusso, Szmulewitz R, Patel S, et al. First-in-Human Study of Mivebresib (ABBV-075), an Oral Pan-Inhibitor of Bromodomain and Extra Terminal Proteins, in Patients with Relapsed/Refractory Solid Tumors. Clinical Cancer Research. 2019;Epub ahead of print.
18. Massie C, Adryan B, Barbosa-Morais N, Lynch A, Tran M, Neal D, et al. New androgen receptor genomic targets show an interaction with the ETS1 transcription factor. EMBO Reports. 2007; 8:871–8.
19. Makkonen H, Jääskeläinen T, Pitkänen-Arsiola T, Rytinki M, Waltering K, Mättö M, et al. Identification of ETS-like transcription factor 4 as a novel androgen receptor target in prostate cancer cells. Oncogene. 2008; 27:4865–76.
20. Kawahara T, Aljarah A, Shareef H, Inoue S, Ide H, Patterson J, et al. Silodosin inhibits prostate cancer cell growth via ELK1 inactivation and enhances the cytotoxic activity of gemcitabine. The Prostate. 2016; 76:744–56.
21. Smith A, Findlay V, Bandurraga S, Kistner-Griffin E, Spruill L, Liu A, et al. ETS1 transcriptional activity is increased in advanced prostate cancer and promotes the castrate-resistant phenotype. Carcinogenesis. 2012; 33:572–80.
22. Yu J, Yu J, Mani R, Cao Q, Brenner C, Cao X, et al. An Integrated Network of Androgen Receptor, Polycomb, and TMPRSS2-ERG Gene Fusions in Prostate Cancer Progression. Cancer Cell. 2010; 17:443–54.

23. Patki M, Chari V, Sivakumaran S, Gonit M, Trumbly R, Ratnam M. The ETS domain transcription factor ELK1 directs a critical component of growth signaling by the androgen receptor in prostate cancer cells. Journal of Biological Chemistry. 2013; 288:11047–65.

24. Rosati R, Patki M, Chari V, Dakshnamurthy S, McFall T, Saxton J, et al. The Amino-terminal Domain of the Androgen Receptor Co-opts Extracellular Signal-regulated Kinase (ERK) Docking Sites in ELK1 Protein to Induce Sustained Gene Activation That Supports Prostate Cancer Cell Growth. Journal of Biological Chemistry. 2016; 291:25983–98.

25. Wolf I, Heitzer M, Grubisha M, DeFranco D. Coactivators and nuclear receptor transactivation. J Cell Biochem. 2008; 104:1580–6.

26. Imberg-Kazdan K, Ha S, Greenfield A, Poultney C, Bonneau R, Logan S, et al. A genome-wide RNA interference screen identifies new regulators of androgen receptor function in prostate cancer cells. Genome Research. 2013; 23:581–91.

27. Khattabi LE, Zhao H, Kalchschmidt J, Young N, Jung S, Blerkom PV, et al. A Pliable Mediator Acts as a Functional Rather Than an Architectural Bridge between Promoters and Enhancers. Cell. 2019; 178:1145–58.

28. Robinson D, Allen EV,. . . ., Sawyers C, Chinnaiyan A. Integrative Clinical Genomics of Advanced Prostate Cancer. Cell. 2015; 161:1215–122.

29. Taylor B, Schultz N, Hieronymus H, Gopalan A, Xiao Y, Carver B, et al. Integrative genomic profiling of human prostate cancer. Cancer Cell. 2010; 18:11–22.

30. Yu S, Wang Y, Yuan H, Zhao H, Lv W, Chen J, et al. Knockdown of Mediator Complex Subunit 19 Suppresses the Growth and Invasion of Prostate Cancer Cells. PLoS One. 2017; 12:e0171134.

31. Bello D, Webber M, Kleinman H, Wartinger D, Rhim J. Androgen responsive adult human prostatic epithelial cell lines immortalized by human papillomavirus 18. Carcinogenesis. 1997; 18:1215–23.

32. Xiong X, Schober M, Tassone E, Khodadadi-Jamayran A, Sastre-Perona A, Zhou H, et al. KLF4, A Gene Regulating Prostate Stem Cell Homeostasis, Is a Barrier to Malignant Progression and Predictor of Good Prognosis in Prostate Cancer. Cell Rep. 2018; 25(11):3006–20 e7. https://doi.org/10.1016/j.celrep.2018.11.065 PMID: 30540935; PubMed Central PMCID: PMC6405286.

33. Paschalis A, Sharp A, Welti J, Neeb A, Raj G, Luo J, et al. Alternative splicing in prostate cancer. Nature Reviews Clinical Oncology. 2018; 15:663–75.

34. Tran C, Ouk S, Clegg N, Chen Y, Watson P, Arora V, et al. Development of a second-generation antiandrogen for treatment of advanced prostate cancer. Science. 2009; 324:787–90.

35. Wu J, Shao C, Li X, Li Q, Hu P, Shi C, et al. Monoamine oxidase A mediates prostate tumorigenesis and cancer metastasis. Journal of Clinical Investigation. 2014; 124:2891–908.

36. Wu JB, Yin L, Shi C, Li Q, Duan P, Huang JM, et al. MAOA-Dependent Activation of Shh-IL6-RANKL Signaling Network Promotes Prostate Cancer Metastasis by Engaging Tumor-Stromal Cell Interactions. Cancer Cell. 2017; 31(3):368–82. https://doi.org/10.1016/j.ccell.2017.02.003 PMID: 28292438.

37. Gaur S, Gross M, Liao C, Qian B, Shih J. Effect of Monoamine oxidase A (MAOA) inhibitors on androgen-sensitive and castration-resistant prostate cancer cells. The Prostate. 2019; 79:667–77.

38. Liao C, Lin T, Li P, Geary L, Chen K, Vaikari V, et al. Loss of MAOA in epithelia inhibits adenocarcinoma development, cell proliferation and cancer stem cells in prostate. Oncogene. 2018; 37:5175–90.

39. Ou X, Chen K, Shih J. Glucocorticoid and androgen activation of monoamine oxidase A is regulated differently by R1 and Sp1. Journal of Biological Chemistry. 2006; 281:21512–25.

40. Liu Y, Gong Z, Sun L, Li X. FOXM1 and androgen receptor co-regulate CDC6 gene transcription and DNA replication in prostate cancer cells. Biochimica et Biophysica Acta—Gene Regulatory Mechanisms. 2014; 1839:297–305.

41. Liu Y, Liu Y, Yuan B, Yin L, Peng Y, Yu X, et al. FOXM1 promotes the progression of prostate cancer by regulating PSA gene transcription. Oncotarget. 2017; 8:17027–37.

42. Yang Y, Yu J. Current perspectives on FOXA1 regulation of androgen receptor signaling and prostate cancer. Genes and Diseases. 2015; 2:144–51.

43. Li Y, Vongsangnak W, Chen L, Shen B. Integrative analysis reveals disease-associated genes and biomarkers for prostate cancer progression. BMC Medical Genomics. 2014; 7:S3 epub.

44. Diao X, Chen X, Pi Y, Zhang Y, Wang F, Liu P, et al. Androgen receptor induces EPHA3 expression by interacting with transcription factor SP1. Oncology Reports. 2018; 40:1174–84.

45. Lu S, Jenster G, Epner D. Androgen induction of cyclin-dependent kinase inhibitor p21 gene: role of androgen receptor and transcription factor Sp1 complex. Molecular Endocrinology. 2000; 14:753–60.

46. Chen Z, Zhang C, Wu D, Chen H, Rorick A, Zhang X, et al. Phospho-MED1-enhanced UBE2C locus looping drives castration-resistant prostate cancer growth. EMBO Journal. 2011; 30:2405–19.

47. Wang Q, Sharma D, Ren Y, Fondell J. A coregulatory role for the TRAP-mediator complex in androgen receptor-mediated gene expression. Journal of Biological Chemistry. 2002; 277:42852–8.

48. True L, Coleman I, Hawley S, Huang C, Gifford D, Coleman R, et al. A molecular correlate to the Gleason grading system for prostate adenocarcinoma. PNAS. 2006; 103:10991–6.

49. Peehl D, Coram M, Khine H, Reese S, Nolley R, Zhao H. The significance of monoamine oxidase-A expression in high grade prostate cancer. Journal of Urology. 2008; 180:2206–11.

50. White T, Kwon E, Fu R, Lucas J, Ostrander E, Stanford J, et al. The monoamine oxidase A gene promoter repeat and prostate cancer risk. The Prostate. 2012; 72:1622–7.

51. Li Q, Yang S, Maeda Y, Sladek F, Sharrocks A, Martins-Green M. MAP kinase phosphorylation-dependent activation of Elk-1 leads to activation of the co-activator p300. EMBO Journal. 2003; 22:281–91.

52. Janknecht R, Nordheim A. MAP kinase-dependent transcriptional coactivation by Elk-1 and its cofactor CBP. Biochemical and Biophysical Research Communications. 1996; 228:831–7.

53. Robinson P, Trnka M, Bushnell D, Davis R, Mattei P, Burlingame A, et al. Structure of a Complete Mediator-RNA Polymerase II Pre-Initiation Complex. Cell. 2016; 166:1411–22.

54. Yuan C-X, Ito M, Fondell J, Fu Z-Y, Roeder R. The TRAP220 component of a thyroid hormone receptor-associated protein (TRAP) coactivator complex interacts directly with nuclear receptors in a ligand-dependent fashion. Proceedings of the National Academy of Sciences. 1998; 95:7939–44.

55. Rasool R, Natesan R, Deng Q, Aras S, Lal P, Effron SS, et al. CDK7 Inhibition Suppresses Castration-Resistant Prostate Cancer through MED1 Inactivation. Cancer Discovery. 2019;Epub ahead of print.

56. Vijayvargia R, May M, Fondell J. A Coregulatory Role for the Mediator Complex in Prostate Cancer Cell Proliferation and Gene Expression. Cancer Research. 2007; 67:4034–41.

57. He G, Hu J, Zhou L, Zhu X, Xin S, Zhang D, et al. The FOXD3/miR-214/MED19 axis suppresses tumour growth and metastasis in human colorectal cancer. British Journal of Cancer. 2016; 115:1367–78.

58. Zhang X, Fan Y, Liu B, Qi X, Guo Z, Li L. Med19 promotes breast cancer cell proliferation by regulating CBFA2T3/HEB expression. Breast Cancer. 2017; 24:433–41.

59. Liu B, Qi X, Zhang X, Gao D, Fang K, Guo Z, et al. Med19 is involved in chemoresistance by mediating autophagy through HMGB1 in breast cancer. Journal of Cellular Biochemistry. 2019; 120:507–18.

60. Xu Y, Liang Z, Li C, Yang Z, Chen L. LCMR1 interacts with DEK to suppress apoptosis in lung cancer cells. Molecular Medicine Reports. 2017; 16:4159–64.

61. Agaësse G, Barbollat-Boutrand L, Sulpice E, Bhajun R, Kharbili ME, Berthier-Vergnes O, et al. A large-scale RNAi screen identifies LCMR1 as a critical regulator of Tspan8-mediated melanoma invasion. Oncogene. 2016; 36:446–57.

62. Sun M, Jiang R, Li J, Luo S, Gao H, Jin C, et al. MED19 promotes proliferation and tumorigenesis of lung cancer. Molecular and Cellular Biology. 2011; 355:27–33.

63. Zhang Y, Li P, Hu J, Zhao L, Li J, Ma R, et al. Role and mechanism of miR-4778-3p and its targets NR2C2 and Med19 in cervical cancer radioresistance. Biochemical and Biophysical Research Communications. 2019; 508:210–6.

64. Ryan MC, Zeeberg BR, Caplen NJ, Cleland JA, Kahn AB, Liu H, et al. SpliceCenter: a suite of web-based bioinformatic applications for evaluating the impact of alternative splicing on RT-PCR, RNAi, microarray, and peptide-based studies. BMC Bioinformatics. 2008; 9:313. Epub 2008/07/22. https://doi.org/10.1186/1471-2105-9-313 PMID: 18638396; PubMed Central PMCID: PMC2491637.

65. Parsons BD, Schindler A, Evans DH, Foley E. A direct phenotypic comparison of siRNA pools and multiple individual duplexes in a functional assay. PLoS One. 2009; 4(12):e8471. Epub 2009/12/31. https://doi.org/10.1371/journal.pone.0008471 PMID: 20041186; PubMed Central PMCID: PMC2793519.

66. Chen EY, Tan CM, Kou Y, Duan Q, Wang Z, Meirelles GV, et al. Enrichr: interactive and collaborative HTML5 gene list enrichment analysis tool. BMC Bioinformatics. 2013; 14:128. https://doi.org/10.1186/1471-2105-14-128 PMID: 23586463; PubMed Central PMCID: PMC3637064.

67. Kuleshov MV, Jones MR, Rouillard AD, Fernandez NF, Duan Q, Wang Z, et al. Enrichr: a comprehensive gene set enrichment analysis web server 2016 update. Nucleic Acids Res. 2016; 44(W1):W90–7. https://doi.org/10.1093/nar/gkw377 PMID: 27141961; PubMed Central PMCID: PMC4987924.

68. Fonseca GJ, Tao J, Westin EM, Duttke SH, Spann NJ, Strid T, et al. Diverse motif ensembles specify non-redundant DNA binding activities of AP-1 family members in macrophages. Nat Commun. 2019; 10(1):414. https://doi.org/10.1038/s41467-018-08236-0 PMID: 30679424; PubMed Central PMCID: PMC6345992.